FINAL DRAFT REPORT

SOF HRVOC emission study at Longview, Texas

John Johansson[1], Johan Mellqvist[1]

Barry Lefer[2], James Flynn[2]

[1] Department of Earth and Space Science, Chalmers University of Technology, Hörsalsvägen 11, SE-41296 Göteborg, E-mail: johan.mellqvist@chalmers.se

[2]Department of Earth and Atmospheric Sciences, University of Houston
4800 Calhoun Rd Houston, TX 77204-5007

This report is based on work funded by the state of Texas through the East Texas Council of Governments (ETCOG) under the technical direction of Northeast Texas Air Care (NETAC)

Date: 2013-06-04

Title: SOF HRVOC emission study at Longview, Texas

Authors: John Johansson, Johan Mellqvist, Barry Lefer, and James Flynn

Department of Earth and Space Science
Chalmers University of Technology
Hörsalsvägen 11
SE-412 96 Göteborg
Sweden

E-mail: johan.mellqvist@chalmers.se

Executive summary

A measurement study was performed in Longview, Texas during the period May 1 to May 11, 2012. The objective of the study was quantify emissions of HRVOCs (Highly Reactive Volatile Organic Compounds) from a large Petrochemical Complex in the Area. The main methods were SOF (Solar Occultation Flux) and Mobile DOAS (Differential Optical Absorption Spectroscopy) which were used to measure ethene, propene, alkanes, NO_2 and SO_2. Both these methods employ open path absorption spectroscopy on solar light from a mobile platform to measure integrated column concentrations, which enables total emission flux calculations on industrial emission plumes.

Similar measurements were performed during a single day in Longview in a 2011 study [Johansson 2011]. Table ES 1 presents the average emissions of ethene, propene and NO_2 from the Petrochemical Complex as measured in that study, in this study and the emissions reported to the 2009 STARS (State of Texas Air Reporting System) emission inventory [STARS]. The average emissions in the 2012 study was significantly lower than in the 2011 study. However, the 2011 study was just a single day of measurements and the results were within the range of emissions seen during the 2012 study. The 2012 study can thus be considered more representative of a longer period of emissions. The measured emissions are, however, still exceeding the emissions inventories by roughly a factor of 2 for ethene and a factor of 6 for propene, while the measured NO_2 emissions are more in line with inventories, considering all NO_x emissions should not be expected to be NO_2 at the typical measurement distance.

Table ES 1 Average emissions measured in 2011 and 2012 compared to emissions reported to the 2009 STARS (State of Texas Air Reporting System) emission inventory. All emission rates in kg/h.

Species	Measurements in 2011	Measurements in 2012	Measurements in 2012 without upsets	STARS emission inventory data 2009
Ethene	452	249	205	113
Propene	282	211	172	32
NO_2	176	118	118	(NO_x) 207

Table of Contents

1. Introduction

A joint measurement study employing researcher from Chalmers University and University of Houston was in the field in Longview, Texas and surrounding areas from May 1-11, 2012. The objective of the study was to measure emission rates, primarily of HRVOCs (Highly Reactive Volatile Organic Compounds), from a large Petrochemical Complex (the Eastman Complex). The methods used were SOF (Solar Occultation Flux) and Mobile DOAS (Differential Optical Absorption Spectroscopy), which are both spectroscopic methods using sun light to measure vertical columns of different species from a mobile platform.

Figure 1 The measurement vehicle housing all the instruments.

HRVOC emissions contribute to photochemical smog and formation of ground level ozone. Several studies in the Houston Area have shown that industrial HRVOC emissions often exceed emission inventories with a factor of 5-10 [Mellqvist 2007, 2008b, 2010; Rappenglück 2008a, 2008b; De Gouw 2009; Wert 2003; Ryerson 2003]. During a measurement study in 2011 [Johansson 2011], one day was spent measuring at the Petrochemical Complex in Longview and large emissions of ethene and propene were found. This study seeks to investigate whether those measurements are representative by sampling on several days and, if possible, to identify portions of the Eastman complex that contribute most to HRVOC emissions.

2. Methods

The main methods used in this project were the two optical remote sensing methods, i.e. the SOF to measure emissions of VOCs (alkenes and alkanes) and Mobile DOAS to measure formaldehyde, NO_2 and SO_2.

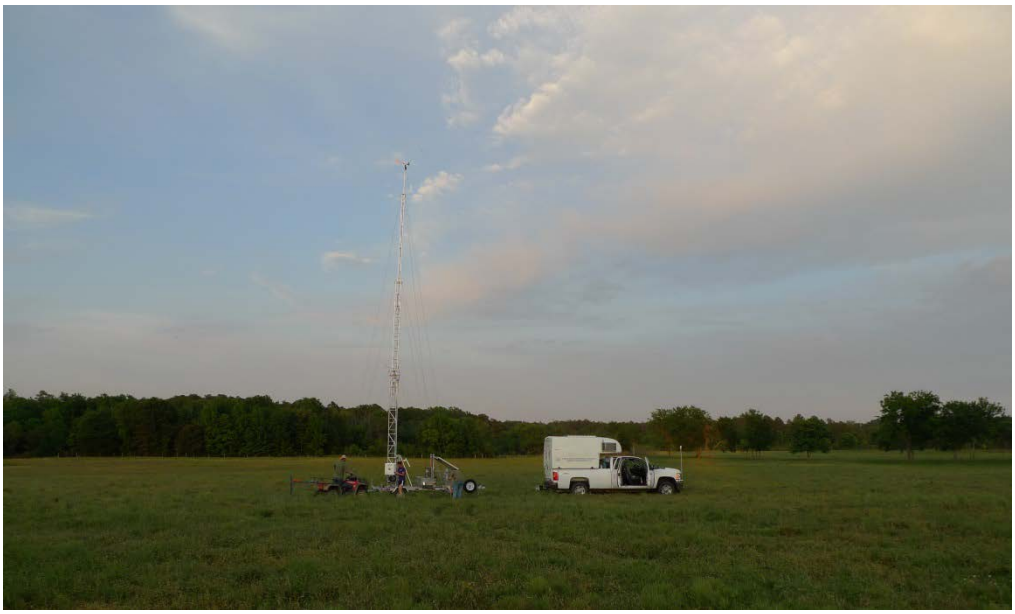

Figure 2. The measurement vehicle with the mobile met tower being deployed.

Figure 3. Overview of the instrument setup on the inside of the measurement vehicle.

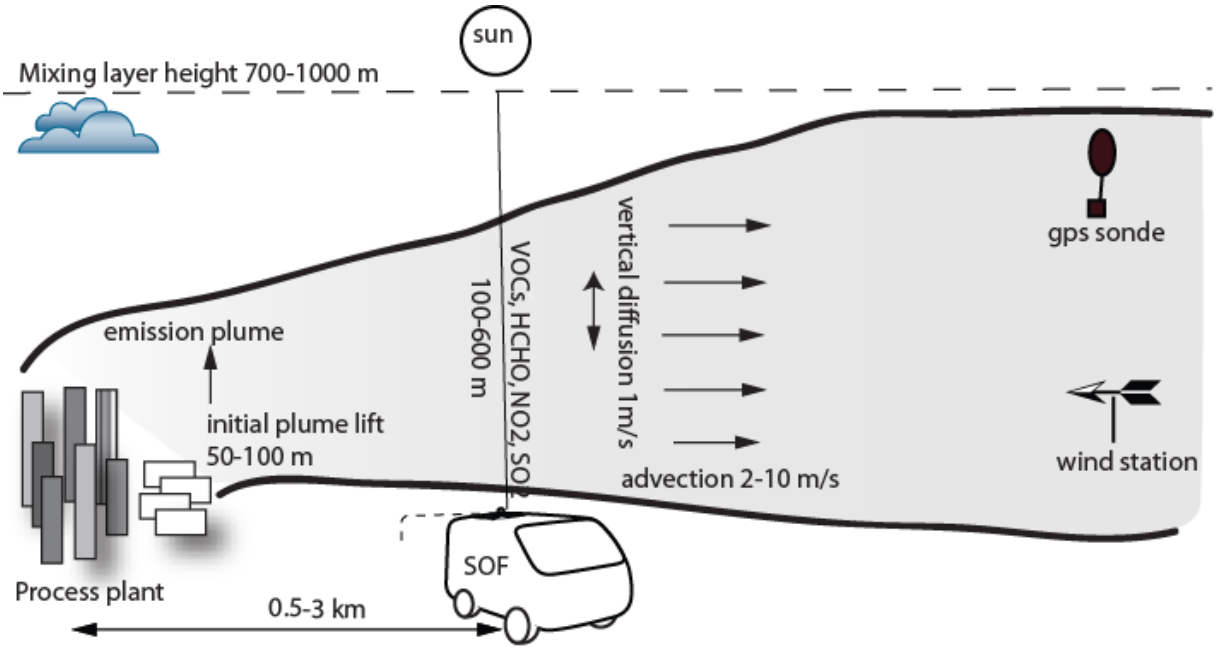

Figure 4. The SOF and Mobile DOAS experiment during the FLAIR campaign is illustrated here. In general the average wind between ground to 500 m was used, obtained from GPS sondes or from up-scaled wind station data. In the measurement car also a Mobile extractive FTIR was operated.

2.1 The SOF method

2.1.1 General

The Solar Occultation Flux (SOF) method is relatively new and was developed from a number of different research projects [Mellqvist 1999a, 1999b; Galle 1999]. The method utilizes the sun as the light source and gas species that absorb in the infrared portion of the solar spectrum are measured from a mobile platform.

The method is today used to screen and quantify VOC emissions from industrial conglomerates down to sub-areas in individual plants. The SOF method is usually combined with an extractive FTIR instrument in the same measurement vehicle, see section 2.3, by which it is possible to carry out complementary measurements, for instance night time measurements of tanks and ship loading operations. Tracer gas is then positioned at the location of the leak and then the ratio of tracer gas and leaking VOC is measured by extracting the gas plume into a gas cell and then analyzing the gas concentrations by infrared spectroscopy.

The SOF method has been applied in several larger campaigns in both Europe and the US and in more than 45 individual plant surveys over the last 7 years. In the various campaign studies it has been found that the measured emissions obtained with SOF are 5–10 times higher than the reported emission obtained by calculations. For instance in a recent study in Houston, TexAQS 2006, it was shown that the industrial releases of alkenes for the Houston Galveston area, on average, were 10 times higher than what was reported [Mellqvist 2010]. These results were supported by airborne measurements [De Gouw 2009]. For alkanes the discrepancy factor was about 8 [Mellqvist 2007]. In a similar study for the conglomerate of refineries and oil storage in the Rotterdam harbor during 2008 [Mellqvist 2009a], a discrepancy factor of 4.4

was found between the alkane measurements and the reported VOC emission values, with individual sites varying between a factor of 2–14. A SOF study, was also carried out in France during 2008 for which large discrepancies were obtained. Also for Swedish refineries the emissions can be considerably higher than calculations and the measurements show that the VOC emissions typically correspond to 0.03–0.09 % of their throughput of oil, with more than half of the emissions originating from oil and product storage [Kihlman 2005a, 2005b].

2.1.2 Details of the method

The SOF method is based on the recording of broadband infrared spectra of the sun with a Fourier transform infrared spectrometer (FTIR) that is connected to a solar tracker. The latter is a telescope that tracks the sun and reflects the light into the spectrometer independent of its position. From the solar spectra it is possible to retrieve the path-integrated concentration (column, see Eq. 1) in the unit mg/m^2 of various species between the sun and the spectrometer. In Figure 5 a measurement system is shown built into a van. The system consists of a custom built solar tracker, transfer optics and a Bruker EM27 FTIR spectrometer with a spectral resolution of 0.5 cm^{-1}, equipped with a combined MCT (mercury cadmium telluride) detector or an InSb (indium antimonide) detector. Optical filters were used to reduce the bandwidth when conducting alkene and alkane measurements.

Figure 5. The SOF system elevated through the roof top of the mobile van. The solar tracker (front left) transmits the solar light into the infrared spectrometer (mid right with a GPS on top) independent of the vehicle's position.

To obtain the gas emission from a source, the car is driven in such way that the detected solar light cuts through the emission plume. This is illustrated in Figure 4 and Figure 7. To calculate the gas emission the wind direction and speed is also required and these parameters are usually measured from high masts and towers.

The spectral retrieval is performed by a custom software, QESOF [Kihlman 2005b], in which calibration spectra are fitted to the measured spectra using a nonlinear multivariate fitting routine. Calibration data from the HITRAN database [Rothman 2003] are used to simulate absorption spectra for atmospheric background species at the actual pressure, temperature and instrumental resolution of the measurements. The same approach is applied for several

retrieval codes for high resolution solar spectroscopy [Rinsland 1991; Griffith 1996] and QESOF has been tested against these with good results. For the retrievals, high resolution spectra of ethene, propene, propane, n-butane, n-octane and other VOCs (e.g. isobutene, 1,3-butadiene) were obtained from the PNL (Pacific Northwest Laboratory) database [Sharpe 2004]. These are degraded to the spectral resolution of the instrument by convolution with the instrument lineshape. The uncertainty in the absorption strength of the calibration spectra is about 3.5 % for the five species.

During the campaign the SOF system was operated mostly in alkene measurement mode, but a separate alkane mode was also used occasionally. The former mode was specifically targeted at ethene and propene and these species were retrieved simultaneously in the wavelength region between 900 and 1000 cm^{-1}, taking into account the interfering species water, CO_2 and ammonia. Ethene is also evaluated separately from propene over a shorter wave number interval. In Figure 6 solar spectra measured inside and outside of a plume downwind of an industrial facility are shown. In addition spectral fits of ethene and propene are shown obtained using the QESOF spectral retrieval algorithm. The fit shown here was evaluated between 900 cm^{-1} and 1000 cm^{-1} to show both ethene and propene. During the campaign the retrievals for ethene, propene and butane had 1σ-variabilities (unsystematic RMS error) in mg/m^2 of about 0.85, 1.15, and 1.73 mg/m^2, respectively, for good measurement conditions over a transect of around 1.5 km with average driving speeds of 30–40 km/h. The variability is caused by interference effects and noise due to instrument vibrations while driving. Under more typical measurement conditions, occasional shadowing, road induced vibration and solar tracking also increase measurement noise. The alkane optical mode is instead based on measurements in the infrared region between 3.3–3.7 μm (2700–3005 cm^{-1}), using the vibration transition in the carbon and hydrogen bond (CH-stretch). The absorption features of the different alkanes are similar and interfere with each other, but since the number of absorbing C-H-bonds is directly related to the molecule mass, the total alkane mass can be retrieved despite the interference. In the analysis we therefore use calibration spectra of propane, n-butane, and n-octane and fit these to the recorded spectra, using a resolution of 8 cm^{-1}. Aromatics and alkenes also have absorption features in the CH-stretch region, but mainly below 3.33 μm for the most abundant species. A sensitivity study of the SOF alkane retrieval was made for the TexAQS 2006 [Mellqvist 2007], taking into account the typical matrix of VOCs, and this study showed that total alkane mass obtained by the SOF was overestimated by 6.6 %. Here we assume the same uncertainty.

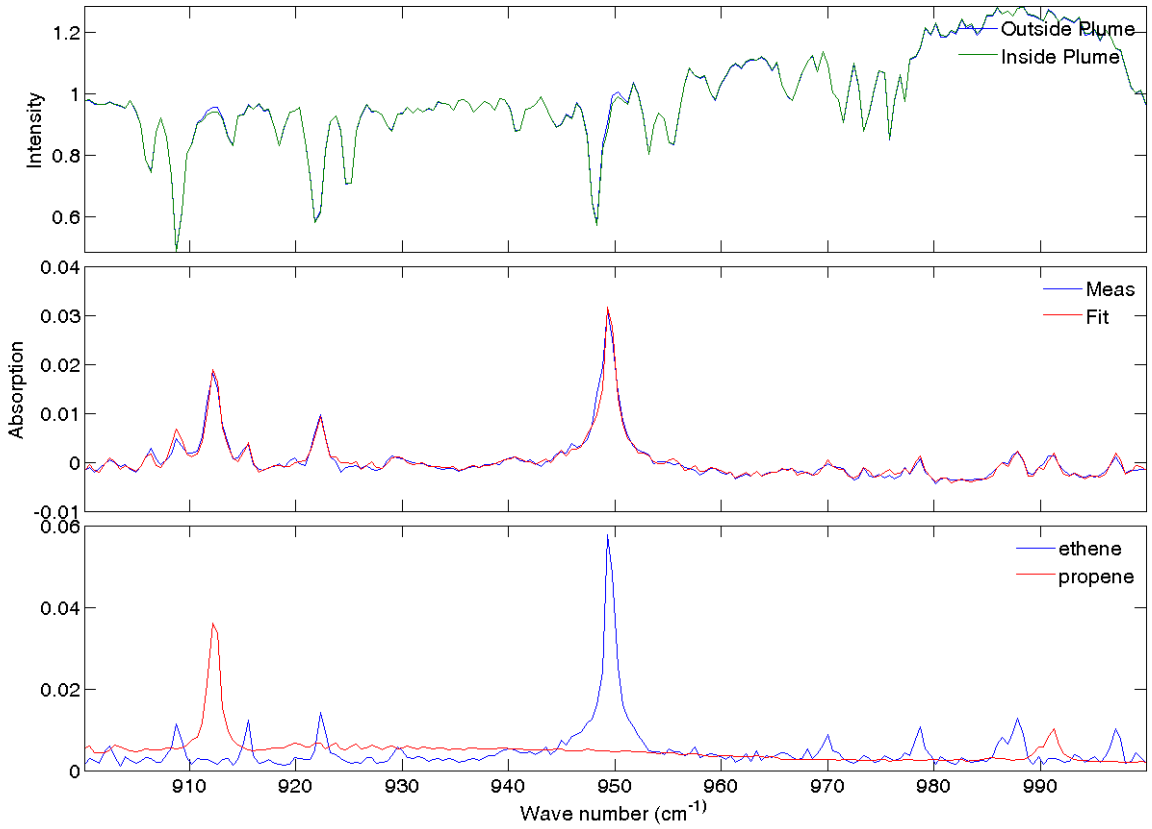

Figure 6. Solar spectra measured outside and inside the emission plume of an industrial plant in arbitrary intensity units (upper). Measured and fitted spectral evaluation for ethene and propene (calibrated spectra, lower) using the QESOF spectral retrieval algorithm is also shown (middle).

2.1.3 Flux calculation

To obtain the gas emission from a target source, SOF transects, measuring vertically integrated species concentrations, are conducted along roads oriented crosswind and close downwind (0.5–3 km) of the target source so that the detected solar light cuts through the emission plume as illustrated in Figure 2. The gas flux is obtained first by adding the column measurements and hence the integrated mass of the key species across the plume is obtained. To obtain the flux this value is then multiplied by the mass average wind speed of the plume, u'_{mw}. The flux calculation is shown in Eq. 1. Here, **x** corresponds to the travel direction, **z** to the height direction, **u'** to the wind speed orthogonal to the travel direction (x), $\mathbf{u'_{mw}}$ to the mass weighted average wind speed and $\mathbf{H_{mix}}$ to the mixing layer height. The slant angle of the sun is compensated for, by multiplying the concentration with the cosine factor of the solar zenith angle.

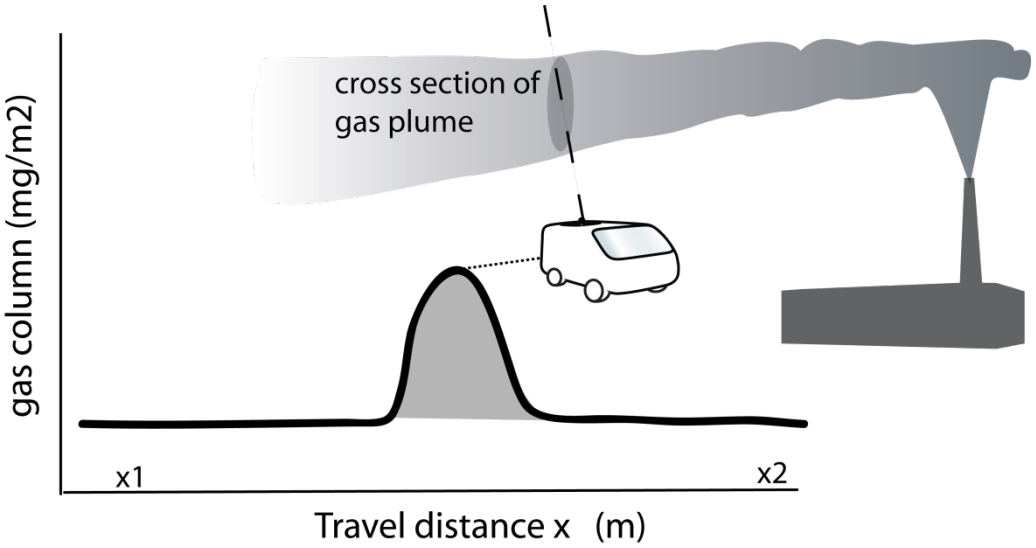

Figure 7. Illustration of the SOF measurement

$$flux = \int_{x1}^{x2}\left(\int_{0}^{Hmix} conc(z)\cdot u'(z)\cdot dz\right)dx = u'_{mw}\int_{x1}^{x2} column(x) \qquad \text{(Eq. 1)}$$

$$\text{where } u'_{mw} = \frac{\int_{o}^{Hmix} conc(z)u'(z)\cdot dz}{\int_{o}^{Hmix} conc(z)dz} \quad \text{and } column = \int_{0}^{Hmix} conc(z)\cdot dz$$

The wind is not straightforward to obtain since it is usually complex close to the ground and increases with the height. The situation is helped by the fact that SOF measurements can only be done in sunny conditions. This is advantageous since it corresponds to *unstable meteorological conditions* for which wind gradients are smoothed out by convection. Over relatively flat terrain with turbulence inducing structures the mean wind varies less than 20 % between 20 and 100 m height using standard calculations of logarithmic wind. This is illustrated for the harbor of Göteborg in Figure 8. Here the average daytime wind velocity and wind direction profile for all sunny days during August of 2004 have been simulated [Kihlman 2005a] using a meteorological flow model denoted TAPM [Hurley 2005].

In addition, for meteorological conditions with considerable convection, the emission plume from an industry mixes rather quickly vertically giving a more or less homogeneous distribution of the pollutant versus height through the mixing layer even a few kilometers downwind. In addition to the atmospheric mixing, the plumes from process industries exhibit an initial lift since they are usually hotter than the surrounding air.

The rapid well-mixed assumption agrees with results from airborne measurements made by NOAA (National Oceanic and Atmospheric Administration) [De Gouw 2009] and Baylor University [Buhr 2006] during the TexAQS 2006 in which also SOF measurements were conducted [Mellqvist 2010]. The NOAA measurements indicate that the gas plumes from the measured industries mix evenly from the ground to 1000 m altitude, i.e. throughout the entire

mixing layer, within 1000–2000 s (~25 min) transport time downwind the industrial plants. This indicates a vertical mixing speed of the plume between 0.5 to 1 m/s. This is further supported by Doppler LIDAR (Light Detection And Ranging) measurements by NOAA showing typical daytime vertical mixing speeds of ±(0.5–1.5) m/s [Tucker 2007].

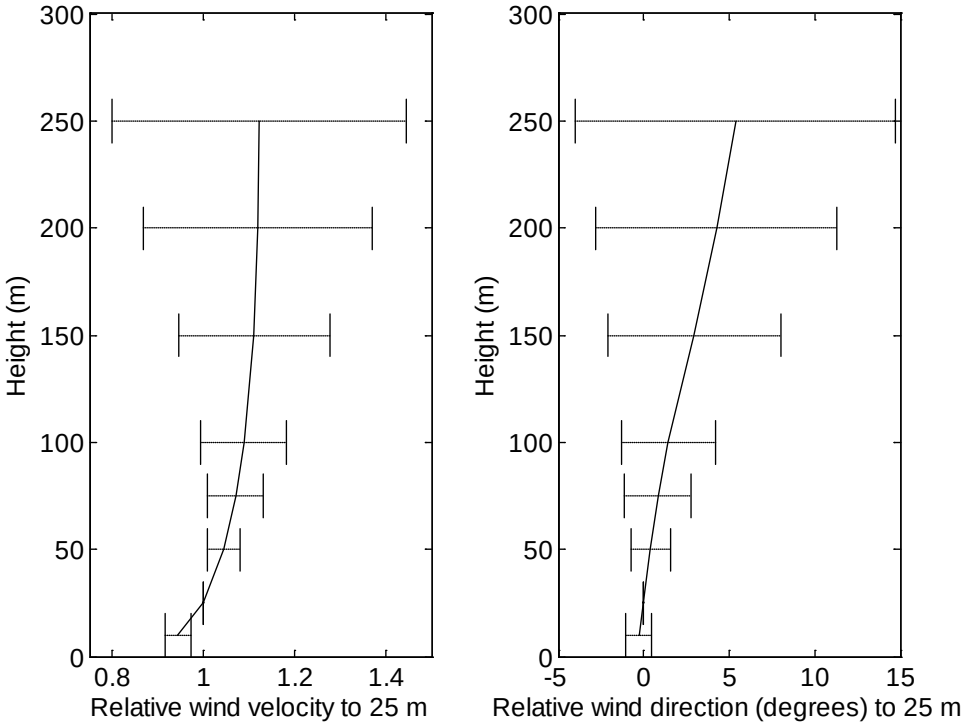

Figure 8. Average daytime wind velocity and wind direction profile retrieved by simulation above Göteborg harbor area averaged over all sunny days during a month with a wind-speed of 3–6 m/s at ground. The error bars indicate standard deviation between daily averages [Kihlman 2005a].

In this study, the measurements were conducted downwind of the industries at a typical plume transport time of 100–1000 s. According to the discussion above this means that the emission plumes have had time to mix up to heights of several hundred meters above the ground, above the first 50–100 m where the wind is usually disturbed due to various structures. For this reason we have used the average wind from 0 to 350 m height in the flux calculations. This wind was measured using GPS balloon sondes launched in the Longview area during the study. These averages were used to scale and verify continuous wind measurements from two ground sites, see section 3.

Figure 9 shows a real measurement example illustrating the principle for the SOF and Mobile DOAS measurements. Here a measurement of alkanes, a transect across the plume downwind of a refinery, is shown. The measured gas column of alkanes in the unit mass/area (mg/m^2), as measured by the SOF in the solar light, is plotted versus distance across the plume. The wind was measured simultaneously by a GPS balloon, in the vicinity of the measurement as shown in Figure 10 and the 0–200 m value corresponds to 7.9 m/s, while the 0–500 value corresponds to 8.4 m/s. In the flux calculation the columns are integrated across the transect, whereby the integrated mass in unit mass per length unit in the plume (mg/m) is obtained. This value corresponds to an average column value of 48 mg/m^2 across the whole transect, over 1300 m. This mass value is then multiplied by the wind speed, to obtain mg/s.

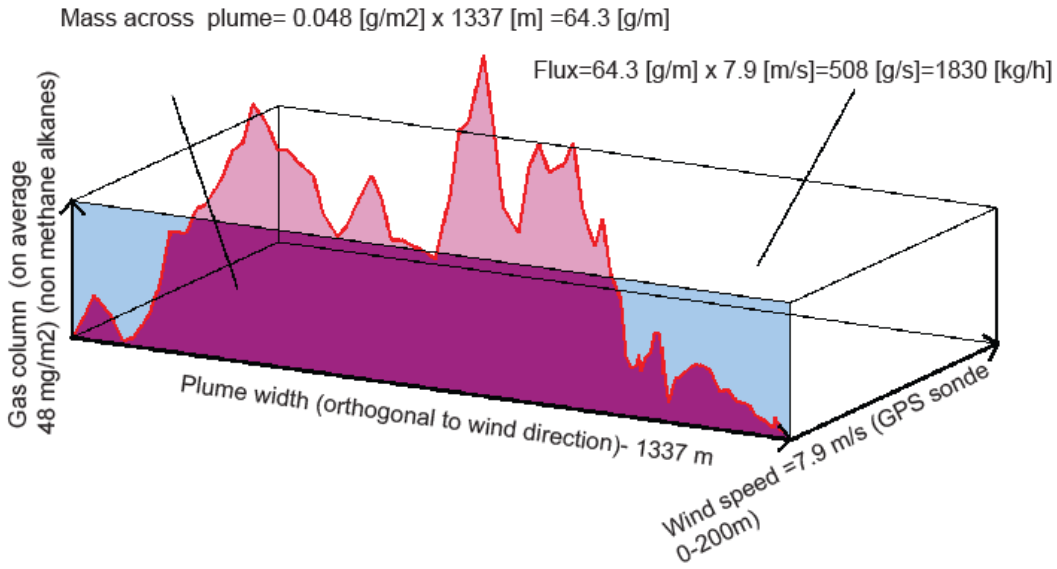

Figure 9. Illustration of the flux calculation in the SOF method for a measurement of alkanes conducted downwind of a refinery. The gas column of alkanes, retrieved from the spectra, is plotted versus distance. In the flux calculation the gas columns are integrated along the measurement transect, corresponding to the lilac area. This area, which is the integrated mass of the plume, corresponds to the same mass as an average column of 48 mg/m^2 integrated along the transect of 1337 m. The integrated mass is then multiplied with the wind speed yielding the flux in mass per seconds. Here an average wind speed from ground to 200 m was used corresponding to 7.9 m/s obtained from the GPS sonde in Figure 10.

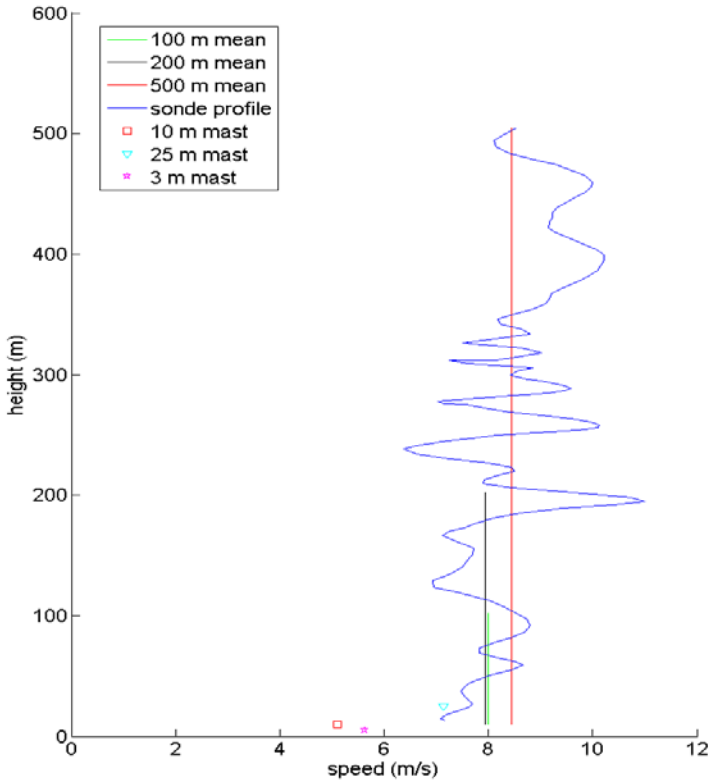

Figure 10. Wind profile measured with a GPS sonde less than ten minutes after the alkane transect shown in Figure 9 above. The wind speed versus height is shown for the balloon measurements in addition to the 0–500 and the 0–200 m average values, and values for several masts at the refinery.

To verify that a measured flux is originating from a specific area upwind of where the emission was detected, another measurement transect needs to be performed upwind of that

area to make sure that the emission is not coming from another source further away. If no significant flux is detected on the upwind side, this measurement does not need to be repeated for every downwind transect. If a smaller flux is measured on the upwind side than on the downwind side, the emission from the area in between is the difference between these fluxes. In this case the upwind transect needs to be repeated with every downwind transect. This type of emission measurements is preferably avoided since it might increase the uncertainty. Upwind measurements were performed at the main measurement site but no significant emissions were detected.

2.2 Mobile DOAS

2.2.1 General

Mobile DOAS (Differential Optical Absorption Spectroscopy) measurements of scattered solar light in zenith direction were carried out in parallel with the SOF measurements, from the same vehicle, in order to measure formaldehyde, NO_2 and SO_2. DOAS works in the ultraviolet (UV) and visible wavelength region while SOF works in the infrared region and hence there are large differences in spectroscopy and in the used spectrum evaluation methods. However, both methods measure vertical columns which are integrated along measurement transects and multiplied by the wind to obtain the flux. The principle of flux-measurements using Mobile DOAS is hence the same as for SOF, section 2.1.3, although it is not necessary to compensate for any slant angle observations since the telescope is always pointing towards zenith. The DOAS system also works under cloudy conditions in contrast to SOF, although the most precise measurements are conducted in clear sky.

The DOAS method was introduced in the 1970's [Platt 1979] and has since then become an increasingly important tool in atmospheric research and monitoring both with artificial light sources and in passive mode utilizing the scattered solar light. In recent time the multi axis DOAS method (scanning passive DOAS) has been applied in tropospheric research for instance measuring formaldehyde [Heckel 2005]. Passive DOAS spectroscopy from mobile platforms has also been quite extensively applied in volcanic gas monitoring [Galle et al., 2002] for SO_2 flux measurements and for mapping of formaldehyde flux measurements in megacities [Johansson 2009]. Mobile DOAS has only been used to a limited extent for measurements of industries; Rivera et al. [2009c] did SO_2 measurements on a power plant in Spain for validation purposes. They also made measurements at an industrial conglomerate in Tula in Mexico [Rivera 2009d] and measurements of SO_2, NO_2 and HCHO during the TexAQS 2006 campaign [Rivera 2009a, 2009b]. There are also groups in both China and Spain working with mobile mini DOAS.

2.2.2. Details of the method

The Mobile DOAS system used in this project, shown in Figure 11 and Figure 12, has been developed for airborne surveillance of SO_2 in ship plumes [Mellqvist 2008a] but has for this project been modified to also measure HCHO and NO_2. It consists of a UV spectrometer (ANDOR Shamrock 303i spectrometer, 303 mm focal length, 300 µm slit) equipped with a CCD (charge-coupled device) detector (Newton DU920N-BU2, 1024 by 255 pixels, thermoelectrically cooled -70^{o}C). The spectrometer has wavelength coverage of 309 to 351 nm and a spectral resolution of 0.63 nm (1800 grooves/mm holographic grating). The spectrometer is connected to a quartz telescope (20 mrad field of view, diameter 7.5 cm) via

an optical fiber (liquid guide, diameter 3 mm). An optical band pass filter (Hoya) is used to prevent stray light in the spectrometer by blocking wavelengths longer than 380 nm.

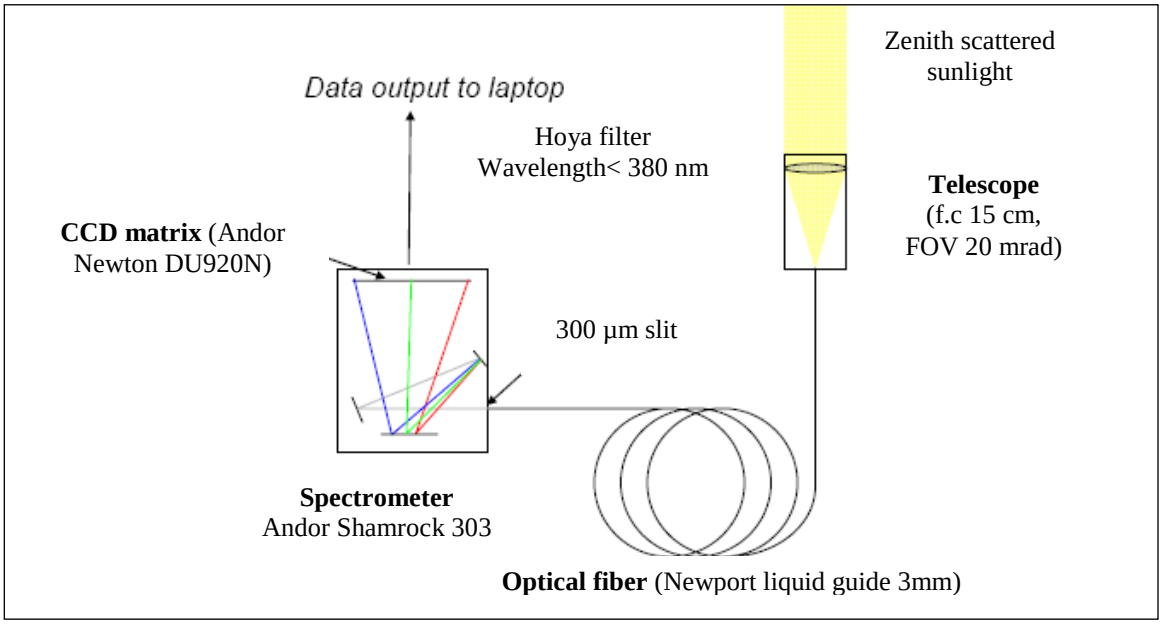

Figure 11. Overview of the Mobile DOAS system used. Scattered solar light is transmitted through a telescope, and an optical fiber to a UV/visible spectrometer. From the measured spectra the amount of HCHO, NO_2 and SO_2 in the solar light can be retrieved.

The DOAS system measures ultraviolet spectra in the 308–352 nm spectral region from which total columns of HCHO, NO_2 and SO_2 can be retrieved, Figure 13. HCHO and NO_2 are retrieved between 324 to 350 nm, together with the interfering species O_3, O_4 and SO_2. SO_2 and O_3 is then retrieved between 310 to 324 nm together with the NO_2 and HCHO columns obtained from the previous retrieval at 324–350 nm, Figure 14.

In the spectral evaluation the recorded spectra along the measurement transect are first normalized against a reference spectrum recorded upwind the industry of interest. In this way most of the absorption features of the atmospheric background and the inherent structure of the sun is eliminated. Ideally the reference spectrum is expected not to include any concentration above ambient of the trace species of interest, however in urban and industrial areas this is difficult to achieve, and therefore our measurement in this case will produce the difference in vertical columns between the reference spectrum and all measured spectra across the plume for every measurement series. The normalized spectra are further high pass filtered according the algorithms proposed by Platt and Perner [1979], and then calibration spectra are scaled to the measured ones by multivariate fitting. Here we have used a software package denoted QDOAS [Van Roozendael 2001] developed at the Belgian Institute for Space Aeronomy (BIRA/IASB) in Brussels.

The calibration spectra used here for the various gases are obtained from the following: HCHO [Cantrell 1990], NO_2 [Vandaele 1998], SO_2 [Bogumil 2003], O_3 [Burrows 1999] and O_4 [Hermans 1999]. In addition to these calibration spectra it is also necessary to fit a so called Ring spectrum, correcting for spectral structures arising from inelastic atmospheric scattering [Fish 1995]. The Ring spectra used have been synthesized with a component of the QDOAS software, which uses a high resolution solar spectrum to calculate the spectrum of Raman scattered light from atmospheric nitrogen and oxygen, convolves this spectrum and the high resolution solar spectrum with the instrument lineshape and calculate the ratio

between them. One problem with the acquired spectra is the fact that the wavelength scale of the spectrometer was variable with shifts in the wavelength scale for the individual spectra. Even though these shifts were minute, within 0.02 nm, they still cause large residuals when normalizing the spectra to the reference spectrum. To overcome this we have used the QDOAS program, to characterize the wavelength calibration of the spectra by comparing the positions of the solar absorption lines with a high-resolved solar spectrum. This improved the results quite considerably. An example of a fit can be seen in Figure 13 in which a calibration spectrum of formaldehyde has been fitted to the measured differential absorbance. This differential spectrum corresponds to a high pass filtered atmospheric spectrum with the features of ozone, NO_2 and spectrum of inelastic atmospheric scattering removed. This spectrum was measured south west of the HSC and corresponds to 3.8 10^{16} molecules/cm^2 as can be seen in Figure 13.

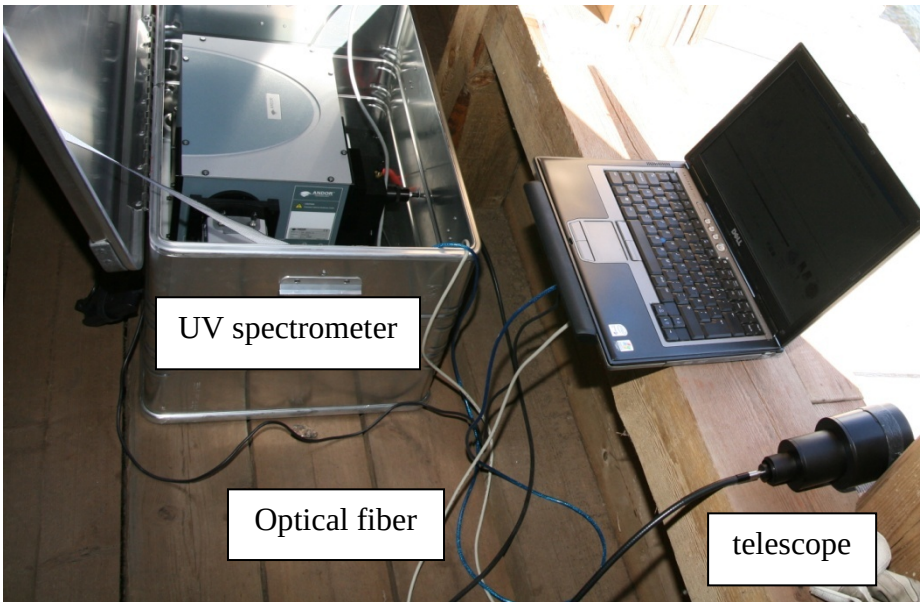

Figure 12. The Mobile DOAS system consisting of a UV spectrometer, optical fiber and UV telescope.

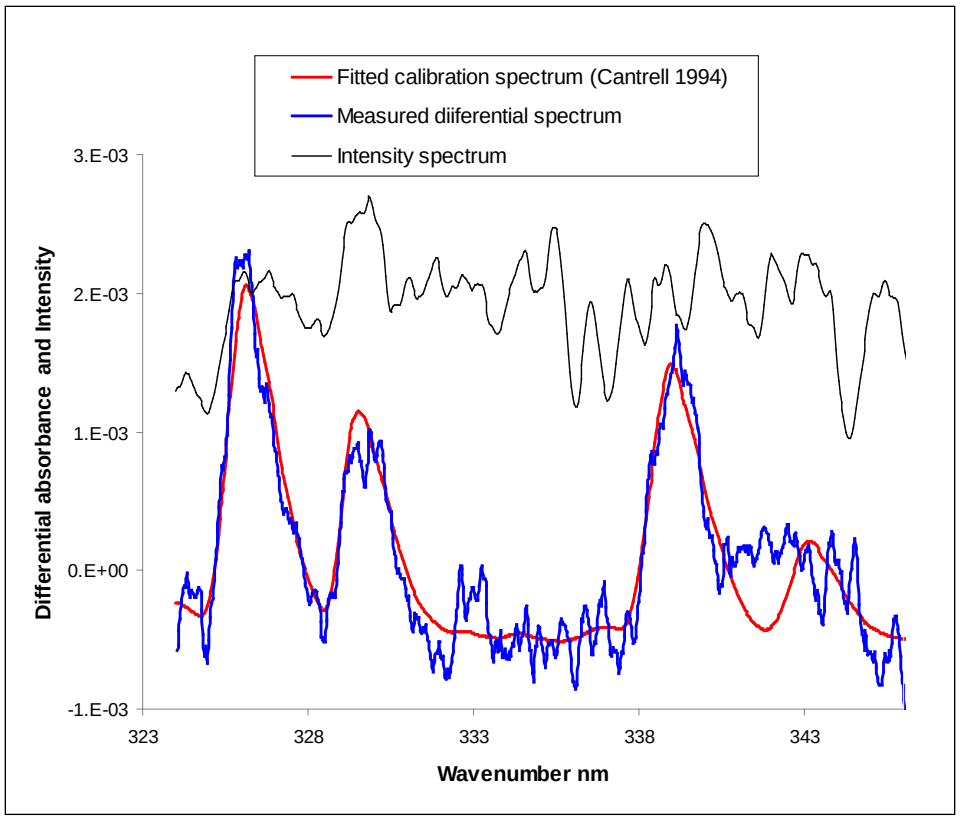

Figure 13. Ultraviolet spectrum (Intensity counts versus wavelength) measured south west of HSC by the Mobile DOAS system on May 20 2009, 10:40, adapted from Mellqvist 2010. From this spectrum a formaldehyde column of 3.8 10^{16} molecules/cm^2 was derived by fitting a calibration spectrum to the measured high pass filtered absorbance (after subtraction of ozone, NO_2 and inelastic atmospheric scattering).

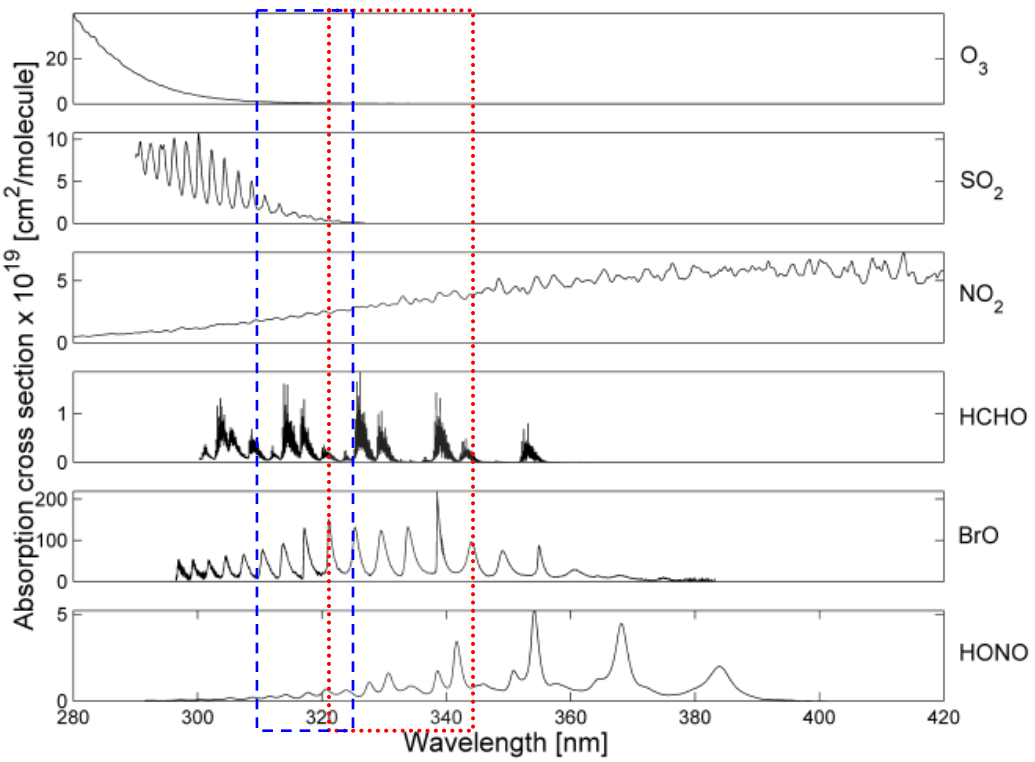

Figure 14**.** Absorption features of formaldehyde and some other interfering species of relevance are shown. The two wavelength regions applied for the retrieval of HCHO (red) and NO_2 (red) and SO_2 (blue), respectively, indicated by the colored rectangles. The above species were retrieved simultaneously, together with oxygen dimer (O_4) and a zenith sky spectrum and a so called ring spectrum.

3. Wind Measurements

Accurate wind measurements are crucial to calculating fluxes from the measured concentration columns. The most accurate and reliable wind measurements for this purpose are achieved with wind-following radiosondes. These are radiosondes with built-in GPS receivers which are launched with helium balloons to track the wind as the balloon follows it. From the data sent back by the radiosonde, a wind profile i.e. wind speed and direction as a function of height, can be reconstructed. Radiosondes, however, only give a snapshot of the wind at the time of launch and the high cost of each launch limits the number of launches that can be made during a measurement campaign. Altogether 10 radiosondes were launched during the Longview campaign. Examples of two wind profiles obtained from radiosonde launches during the campaign can be seen in Figure 15.

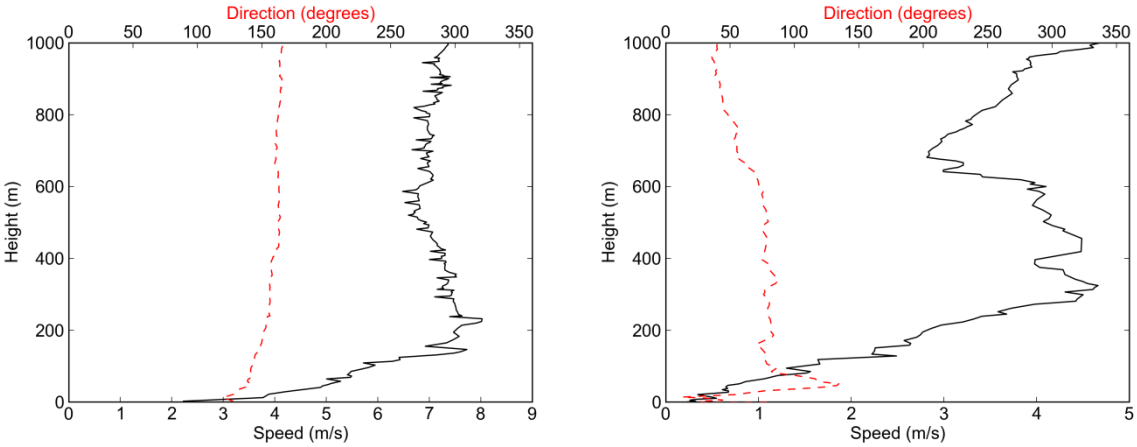

Figure 15 Wind profiles measured with radiosondes. The left profile is from a sonde launched northeast of the Petrochemical Complex at 18:16 on May 3. The right profile is from a sonde launched southwest of the Petrochemical Complex at 15:23 on May 9.

The wind profiles are averaged over the height interval in which the plume is assumed to be distributed to obtain a mean plume speed. Since we lack specific information about the height distribution of the plumes, the plume is assumed to typically be well mixed from the ground up to somewhere between 200 m and 500 m. This estimation was based on the typical distance from sources to measurement point during the campaign (1-3 km), typical wind speeds during the campaign (2-6 m/s) and typical vertical mixing speeds during sunny conditions (0.5-1 m/s).

Since radiosonde measurements were sparse, they were not employed directly for flux calculations. Instead continuous wind measurements with high temporal resolution from ground masts were used. The wind speeds from these masts were, however, multiplied by a factor to compensate for ground wind speeds generally being lower. These factors were determined by comparing 0-350 m averages (350 m being the average of 200 m and 500 m) of radiosonde wind profiles to simultaneous ground mast measurements. These comparisons were also used to quantify the accuracy of using the ground mast measurements as a proxy for winds higher up.

Figure 16 and Figure 17 shows scatter plots of comparisons between radiosonde wind profile averages (x-axis) and simultaneous ground mast measurements. The two ground masts were a 5 m high mast at the TCEQ operated CAM sites C19, near East Texas Regional Airport, and a 15 m mobile met tower set up on a field southwest of the Petrochemical Complex. The mobile met tower was equipped with two wind meters, one at 15 m and one at 5 m. The wind speeds

were multiplied with a factor so that their average would be the same as for the wind profiles. These factors were 1.33 for the 15 m met tower wind speed, and 1.56 for both the C19 and the 5 m met tower wind speeds.

Table 1 summarizes the uncertainty in using these ground mast wind data as proxies for higher winds. The wind speed error is one standard deviation of the relative difference between mast and sonde wind. The wind direction error is the mean of the absolute difference between mast and sonde wind plus/minus one standard deviation.

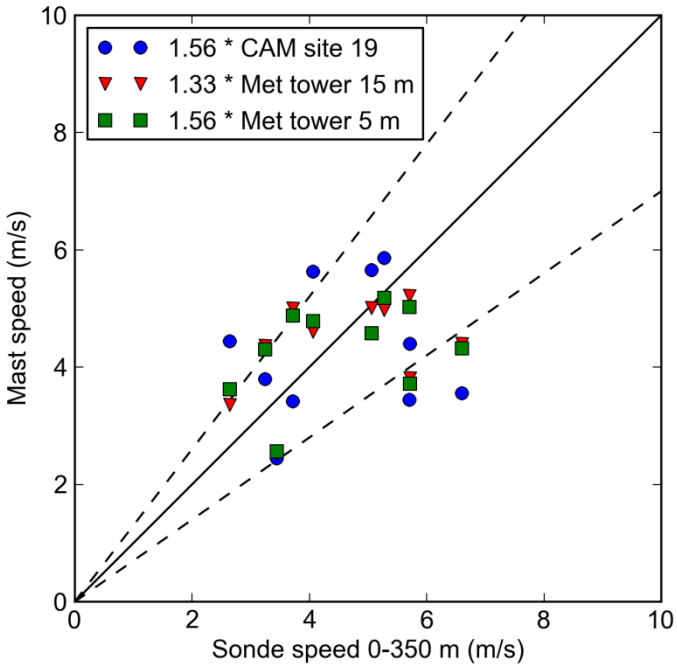

Figure 16 Comparison between wind speed from scaled mast measurements and 0–350 m averages of radiosonde profiles. The dashed lines indicate ±30 % boundaries.

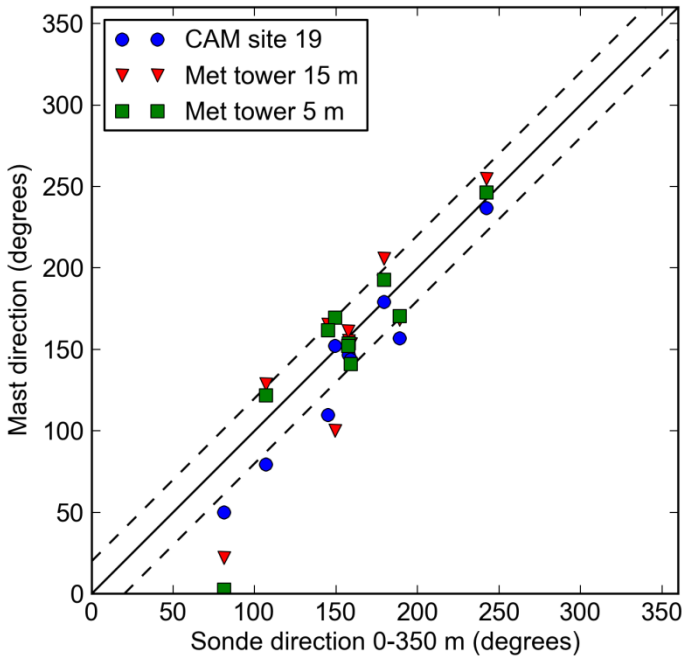

Figure 17 Comparison between wind direction from scaled mast measurements and 0–350 m averages of radiosonde profiles. The dashed lines indicate ±20° boundaries.

Table 1. Statistical differences between 0 to 500 m averages of wind data from sondes launched in Longview and simultaneous TCEQ CAMS mast measurements.

Wind measurement	**Relative difference in speed compared to radiosonde 0-350 m (Relative error)**	**Difference in direction compared to radiosonde 0-350 m**
CAM site C19	±34 %	-16±14°
Met tower 15 m	±25 %	-5±28°
Met tower 5 m	±27 %	-6±28°

4. Measurement uncertainty and quality assurance

4.1 SOF

4.1.1. Measurement uncertainty SOF and Mobile DOAS

The main uncertainty for the flux measurements in the SOF and Mobile DOAS measurements comes from the uncertainty in the wind field. From the wind speed data in Table 1 the 1σ spread relative to the 0–350 m GPS sonde wind is 25–34 %. This error is seen as a measure of the uncertainty in wind speed when calculating fluxes from the measured concentration columns. The wind direction is also associated with an uncertainty, and this error actually depends on how orthogonal the plume is to the transect being conducted. When the plume transect is orthogonal to the wind direction an uncertainty in the wind direction affect the flux uncertainty much less than for more oblique transect angles. A 11–24º wind direction uncertainty (1σ) is estimated for the measurements, from the wind direction errors in Table 1, giving an average of 18 º. This implies a 6 % flux uncertainty at an orthogonal plume transect, and 9 % on average for the transect angle of 75º.

The absorption line parameters of the retrieved compounds are well established in published databases, stating an uncertainty of 3–3.5 % for the spectroscopic part for the VOCs [Sharpe 2004]. For the UV cross section the NO_2 is stated as 4 % [Van Daele 1998]. To the error we have also added a retrieval uncertainty of 10–20 %. This is the combined effect of instrumentation and retrieval stability on the total columns for a plume transect [Mellqvist 2009a]. Also affecting the uncertainty is the error in the SOF alkane mass retrieval due to interference of various compounds in the plume mixture (6 %). The composite flux measurement uncertainty for the SOF measurements, obtained as the square root sum of the quadratic errors for the parameters described above, is 29-37 % for ethene, see Table 2.

Table 2 Uncertainty estimation of the flux measurements (the variability of the sources not taken into account).

	Wind Speed [a)]	**Wind Direct** [b)]	**Spectroscopy (cross sections)** [c)]	**Retrieval error** [d)]	**Composite flux measurement uncertainty** [e)]
Alkanes	25–34 %	6–9 %	3.5 %	12 %	29–37 %
Ethene	25–34 %	6–9 %	3.5 %	10 %	28–37 %
Propene	25–34 %	6–9 %	3.5 %	20 %	33–41 %
SO2	25–34 %	6–9 %	2.8 %	10 %	28–37 %
NO2	25–34 %	6–9 %	4 %	10 %	28–37 %

a) Comparing mast wind averages with the 0–350 m GPS sonde averages, the max data spreads 16–30 % (1σ, 30 %)
b) The 1σ deviation among the wind data compared to the 0–350 m sonde is 18º. For a plume transect orthogonal to the wind direction, which is always the aim, this would give a 6 % error. For a measurement in 75º angle the error is 9 %.
c) Includes systematic and random errors in the cross section database.
d) The combined effects of instrumentation and retrieval stability on the retrieved total columns during the course of a plume transect and error of the SOF alkane mass retrieval. Estimated for SOF.
e) The composite square root sum of squares uncertainty

4.1.2 Validation and comparisons

The performance of the SOF method has been tested by comparing it to other methods and tracer gas release experiments. In one experiment, tracer gas (SF_6) was released from a 17 m high mast on a wide parking lot. The emission rate was then quantified by SOF measurements

50–100 m downwind the source, yielding a 10 % accuracy for these measurements when averaging 5–10 transects [Kihlman 2005b].

More difficult measurement geometries have also been tested by conducting tracer gas releases of SF_6 from the top of crude oil tanks. For instance, in an experiment at Nynas refinery in Sweden tracer gas was released from a crude oil tank. In this case, for close by measurements in the disturbed wind field at a downwind distance of about 5 tank heights, the overestimation was 30 %, applying wind data from a high mast [Kihlman 2005a; Samuelsson 2005b].

The SOF method has also been compared against other methods. In another experiment at the Nynas refinery a fan was mounted outside the ventilation pipe, sucking out a controlled VOC flow from the tank. The pipe flow was measured using a so called pitot pipe and the concentration was analyzed by FID (Flame ionization detector) which made it possible to calculate the VOC emission rate, which was 12 kg/h. In parallel, SOF measurements were carried out at a distance corresponding to a few tank heights, yielding an emission rate of 9 kg/h, a 26 % underestimation in this case. Similar measurements from a joint ventilation pipe from several Bitumen cisterns yielded a FID value of 7 kg/h and only 1 % higher emission from the SOF measurements [Samuelsson 2005b].

During the TexAQS 2006 the SOF method was used in parallel to airborne measurements of ethene fluxes from a petrochemical industrial area in Mont Belvieu [De Gouw 2009]. The agreement was here within 50 % and in this case most of the uncertainties were in the airborne measurements. The SOF method has not been directly compared to the laser based DIAL method (Differential Absorption LIDAR) [Walmsley 1998] which is commonly used for VOC measurements. Nevertheless, measurements at the same plant in Sweden (Preem refinery) yield very similar results when measuring at different years. Differences have been seen for bitumen refineries however [Samuelsson 2005b]. Rivera et al. [2009] did Mobile DOAS measurements of SO_2 on a power plant in Spain and the average determined flux with the DOAS came within 7 % of the values monitored at the plant measurements. All in all the experiment described above is consistent with an uncertainty budget of 20–30 %.

4.1.3. Quality assurance

A formalized QA/QC protocol has not yet been adopted for the SOF method or for Mobile DOAS. However, the spectroscopic column concentration measurements is basically the same as a long path FTIR measurement through the atmosphere corresponding to an effective path length of about 5 km for atmospheric background constituents. For such measurements, there is an EPA guidance document (FTIR Open-Path Monitoring Guidance Document," EPA-600/R-96/040, April 1996).
In addition the US-EPA has developed a test method (OTM 10, Optical Remote Sensing for Emission Characterization from Non-Point Sources), [Thoma 2009] for fugitive emission of methane from landfills. This method is based on measuring the gas flux by integrating the mass across the plume and then multiplying with the wind speed. The mass is here measured by long path FTIR or tuneable diode lasers. The OTM 10 is hence quite similar to the SOF method, since it uses long path FTIR but more importantly since it determines the flux in the same principal manner. The spectral retrieval code used in the SOF method (QESOF) [Kihlman 2005a] relies on principles adopted by the NDACC community (Network for the detection of atmospheric composition change. www.ndsc.ncep.noaa.gov), which is a global

scientific community in which precise solar FTIR measurements are conducted to investigate the gas composition changes of the atmosphere. Chalmers University is a partner of this community and has operated a solar FTIR in Norway since 1994. The QESOF code has been evaluated against several published codes developed within NDACC with good agreement, better than 3 %.

Even though a formalized QA/QC protocol is missing there are several QA procedures carried out prior to conducting the SOF measurements. This includes checking the instrumental spectral response (usually done by measuring solar spectra and investigating the width and line position of these) and investigating that the instruments measures in the same manner, independent of the direction of the instrument relative to the sun. Usually the instrument is aligned to have the same light response in all directions.

The FTIR instrument, used in SOF, is not calibrated prior to measurements but one instead relies on calibration data from the scientific literature. This is appropriate as long as the instrument is well aligned, and whether the alignment has been sufficient can actually be checked afterwards by investigating the widths and shape of the absorption lines in the measured solar spectra.
Noteworthy is the fact that the spectra are stored in a computer and that the spectral analysis is conducted afterwards which makes it possible to conduct quality control on the data. From this analysis the individual statistical error is obtained for each measurement. Quality control is also conducted by removing "bad" spectra".

For open path DOAS standardization work is carried out which is very similar to this application from a spectroscopic point of view. For instance the US EPA has tested several long path instruments within their environmental technology verification program with good results.

The spectral evaluation used in this study is similar to many other studies since we rely on a software package widely used by the DOAS community (QDOAS) and we use published calibration reference data. The most important issue when it comes to quality assurance is to investigate the lineshape of the spectrometer and the wavelength calibration. During the campaign this was done by regular measurement with a low pressure Hg calibration lamp. The wavelength calibration was also corrected afterwards by comparing the measured spectra to a solar spectrum, and then shifting them accordingly to the difference.
The quality of the data can be checked by investigating the spectral fitting parameters and in this way remove bad data.

5. Results of Measurements

Figure 18 shows the locations of the Petrochemical Complex as well as three nearby power plants. Although the Petrochemical Complex was the focus of the study, occasional measurements were done at the power plants to assess possible measurement interference. The results of the measurements at the Petrochemical Complex are presented below.

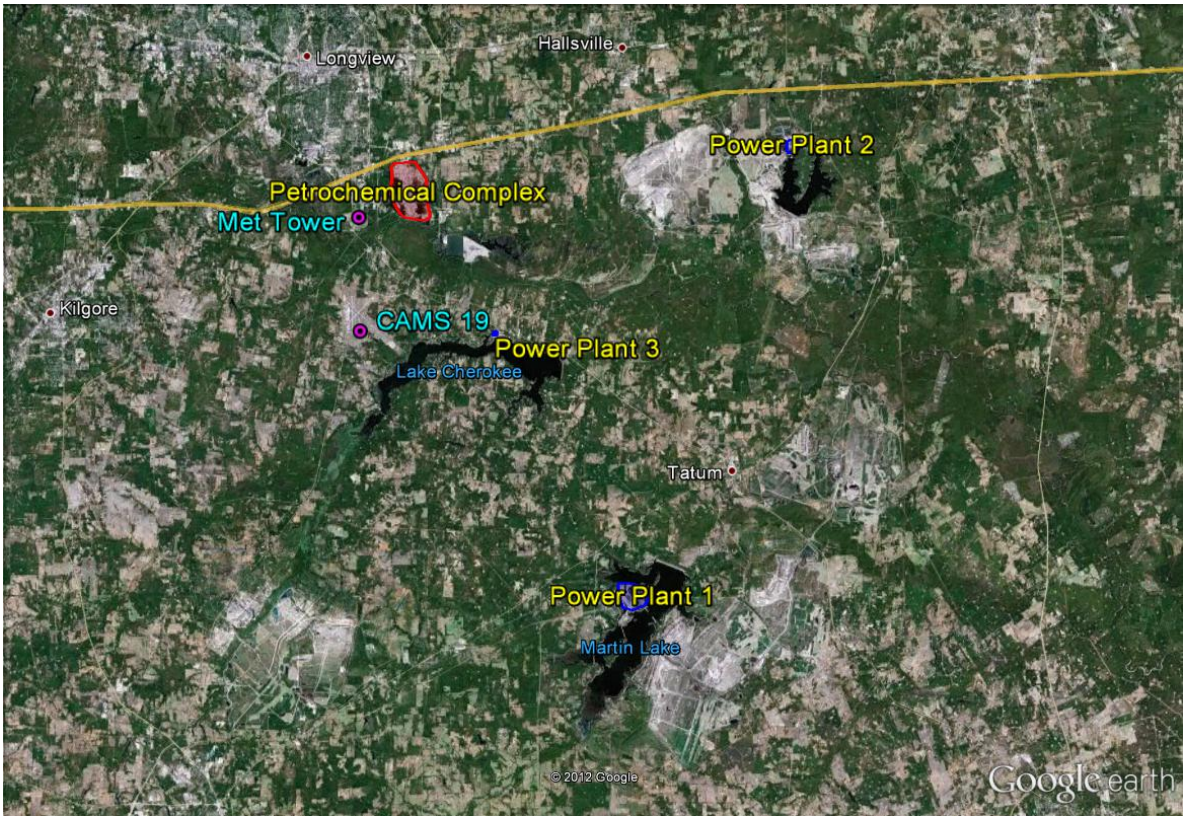

Figure 18 Map showing the locations of the measurement sites visited during the campaign and the ground masts used for flux calculations. The Petrochemical Complex (PC) was the main focus, but plumes from nearby power plants (PP1-PP3) were sometimes encountered.

5.1 Petrochemical Complex

Since the Petrochemical Complex was the main focus of the campaign most of the time was spent measuring downwind of it or waiting close by for weather conditions to improve. The dominating weather pattern during the period was southerly wind and partially cloudy skies which occasionally cleared for a couple of hours, mostly in late afternoon/evening. This was generally enough to make it possible to make at least a few SOF measurements every day. May 8 saw a frontal passage with more cloud coverage and culminating in a thunderstorm which was followed by longer streaks of clear skies and southeasterly and easterly winds on May 9 and 10.

5.1.1 Alkenes

Ethene and propene were the primary species of interest during the campaign. Since southerly winds dominated, most measurements were of fairly narrow plumes, sometimes with a longer tail in one direction, intercepted along the access road adjacent to Interstate 20, north of the

Complex. However, a brief period of southwesterly winds on May 7 and wind directions ranging from northeasterly to southeasterly on May 9 and May 10 provided for some complementary measurement scenarios. The ethene and propene plumes were mostly co-located, but some spatial separation could be seen at times. A selection of measurement traverses representing most wind directions are shown in Figure 20 to Figure 23.

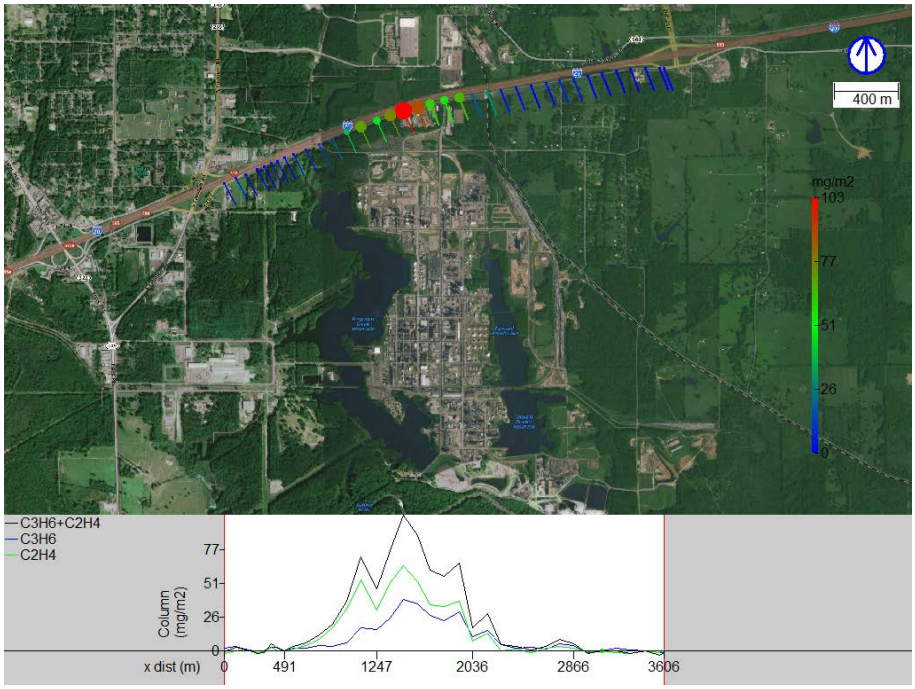

Figure 19 SOF measurement of ethene and propene north of the Petrochemical Complex on May 3, 2012, 17:29. Each measured spectrum is represented with a point, which color and size indicate the evaluated integrated vertical column of ethene and propene. The ethene (green line), propene (blue line) and total (black line) columns by distance driven through the plume is also shown in the lower part of the figure. A line from each point indicates the direction from which the wind is blowing.

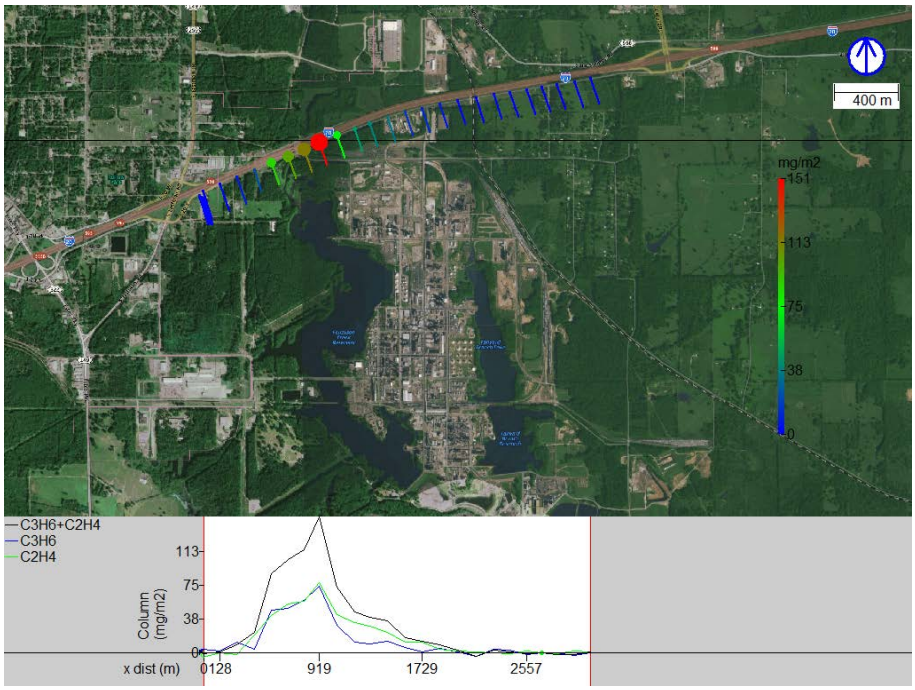

Figure 20 SOF measurement of ethene and propene north of the Petrochemical Complex on May 7, 2012, 08:26. Each measured spectrum is represented with a point, which color and size indicate the evaluated integrated vertical column of ethene and propene. The ethene (green line), propene (blue line) and total (black line) columns by distance driven through the plume is also shown in the lower part of the figure. A line from each point indicates the direction from which the wind is blowing.

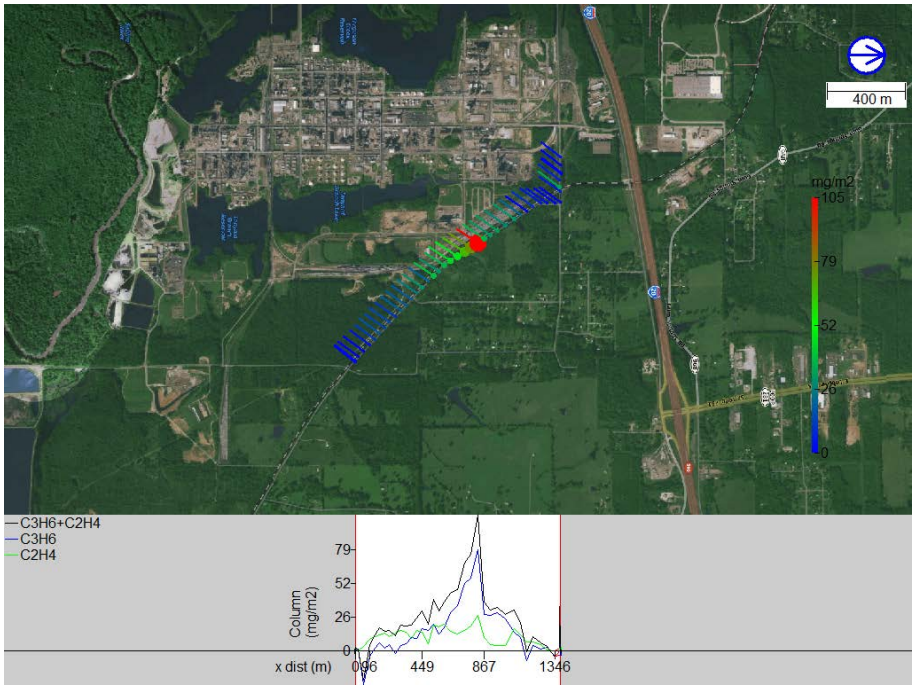

Figure 21 SOF measurement of ethene and propene east of the Petrochemical Complex on May 7, 2012, 11:28. Each measured spectrum is represented with a point, which color and size indicate the evaluated integrated vertical column of ethene and propene. The ethene (green line), propene (blue line) and total (black line) columns by distance driven through the plume is also shown in the lower part of the figure. A line from each point indicates the direction from which the wind is blowing.

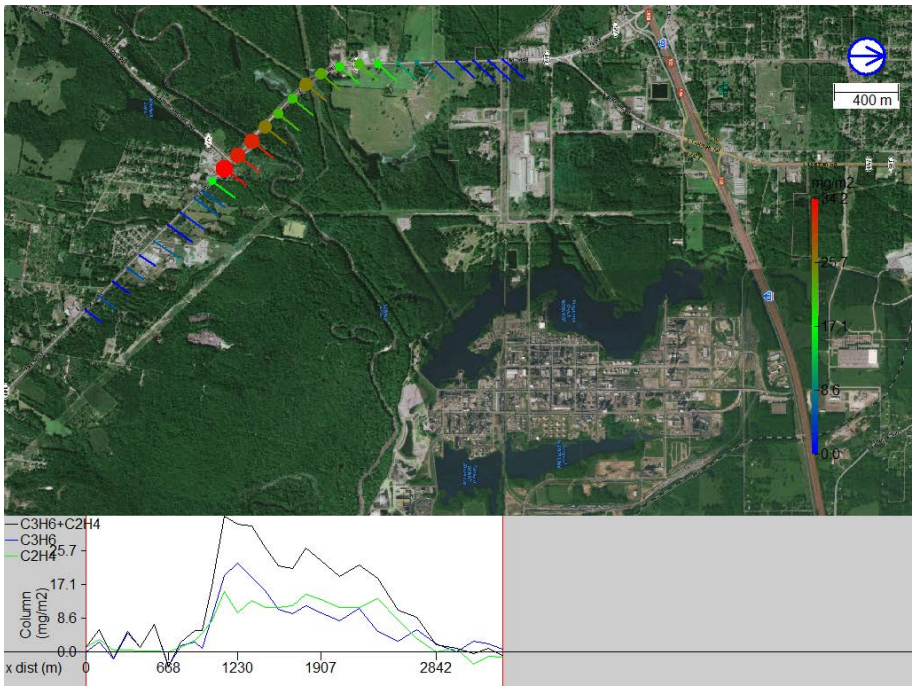

Figure 22 SOF measurement of ethene and propene southwest of the Petrochemical Complex on May 9, 2012, 14:23. Each measured spectrum is represented with a point, which color and size indicate the evaluated integrated vertical column of ethene and propene. The ethene (green line), propene (blue line) and total (black line) columns by distance driven through the plume is also shown in the lower part of the figure. A line from each point indicates the direction from which the wind is blowing.

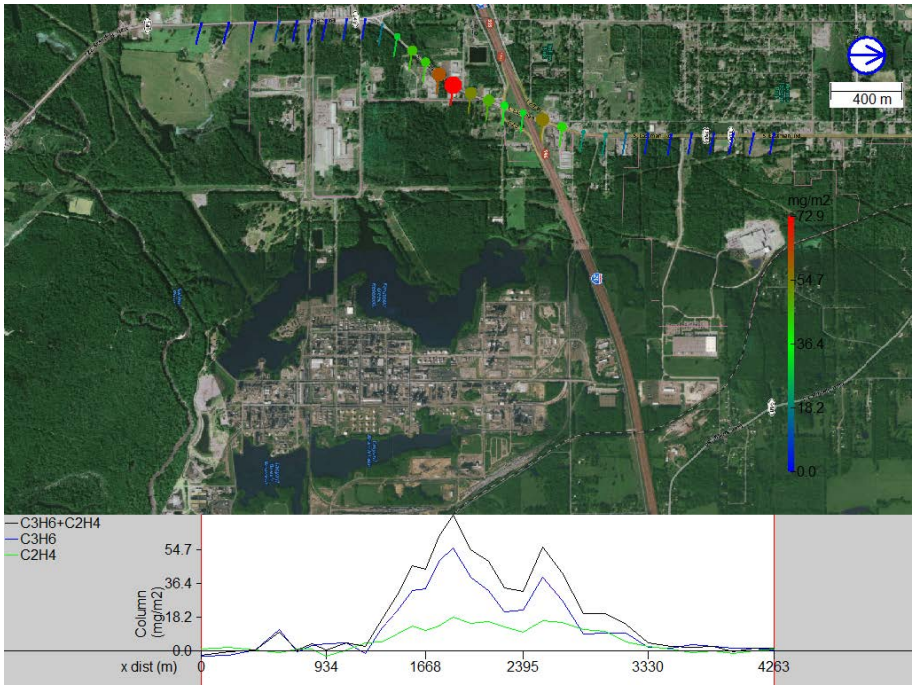

Figure 23 SOF measurement of ethene and propene west of the Petrochemical Complex on May 10, 2012, 11:33. Each measured spectrum is represented with a point, which color and size indicate the evaluated integrated vertical column of ethene and propene. The ethene (green line), propene (blue line) and total (black line) columns by distance driven through the plume is also shown in the lower part of the figure. A line from each point indicates the direction from which the wind is blowing.

The results of all successful ethene and propene traverses are summarized in Table 3 and Table 4 respectively. Altogether, there were 67 successful ethene traverses and 60 successful propene traverses, distributed over 8 days. Propene evaluations are more sensitive to disturbances, such as vibrations and low light intensities, and hence some traverses were usable for ethene but not for propene. This is why there are less traverses for propene than for ethene. The average emission rate for all traverses were 249 kg/h of ethene and 211 kg/h of propene, with standard deviations of 130 kg/h and 122 kg/h respectively.

Table 3 Summary of ethene emission transects from the Petrochemical Complex. N is the number of traverses, Start and Stop are start and stop times in HHMMSS, Mean and SD are the average and standard deviation of the calculated fluxes and WS and WD are wind speed and wind direction.

Region	Day	N	Start	Stop	Mean (kg/h)	SD (kg/h)	WS (m/s)	Range WD (deg)	
PC									
	120502	11	142455	181749	160.6	64.9	2.3	149	227
	120503	5	170946	185159	248.0	52.3	2.8	143	167
	120504	3	115940	182805	210.6	23.4	3.0	155	176
	120505	9	134649	181145	224.2	76.1	3.7	134	175
	120506	4	110736	164908	192.1	49.1	3.9	155	210
	120507	22	82936	181932	334.6	184.2	2.7	161	221
	120509	5	114323	145704	218.4	44.1	3.4	24	64
	120510	8	100805	120749	224.6	24.0	2.4	98	155
Total		**67**	**82936**	**185159**	**248.9**	**129.8**	**2.9**	**24**	**227**

Table 4 Summary of propene emission transects from the Petrochemical Complex.

Region	Day	N	Start	Stop	Mean (kg/h)	SD (kg/h)	WS (m/s)	Range WD (deg)	
PC									
	120502	10	143943	181439	227.7	128.1	2.3	150	228
	120503	5	171001	185115	132.8	37.3	2.8	143	166
	120504	2	120305	174545	186.3	4.8	3.3	161	175
	120505	9	134733	181101	175.7	72.6	3.7	134	176
	120506	4	110849	164853	147.0	24.7	3.9	155	211
	120507	17	82906	182016	155.3	54.1	2.7	161	221
	120509	5	114309	145650	212.9	55.6	3.4	24	65
	120510	8	100820	120606	436.2	118.1	2.4	97	155
Total		**60**	**82906**	**185115**	**211.3**	**121.8**	**2.9**	**24**	**228**

The day to day variations were generally small. There were, however, a couple of episodes that broke the uniform pattern. On May 7, the ethene flux suddenly went from normal levels to almost 1000 kg/h in one traverse around noon and remained unusually high for the rest of the day. The propene and NO_2 emissions did not change noticeably, making it hard to explain it as overestimation of the wind speed. Similarly, propene emission were unusually high during the whole day of May 10 without similar changes in ethene or NO_2. These two episodes might be considered upset emissions, perhaps due to temporary emission events.

5.1.2 Alkanes

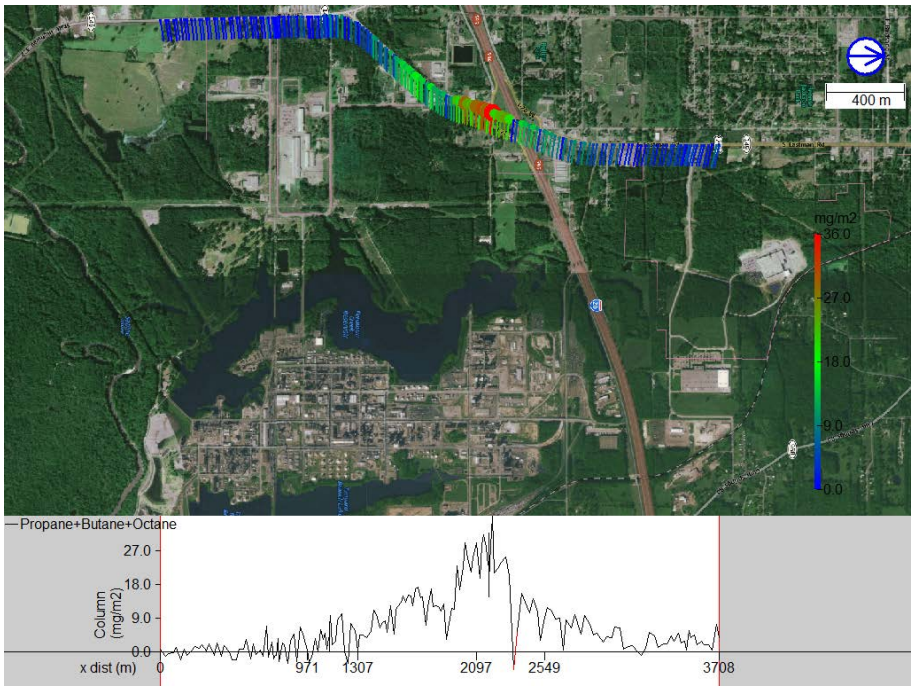

Figure 24 SOF measurement of alkanes west of the Petrochemical Complex on May 10, 2012, 14:14. Each measured spectrum is represented with a point, which color and size indicate the evaluated integrated vertical alkane column. The alkane column by distance driven through the plume is also shown in the lower part of the figure. A line from each point indicates the direction from which the wind is blowing.

Although ethene and propene was of main interest due to their high reactivity, there were some attempts at alkane measurements in the last days of the campaign. Alkane measurements require some instrument adjustments and realignment of the optical setup for which there was not enough time to do rigorously. This resulted in lower quality of the spectra recorded and less reliable evaluations. For this reason, several traverses were unusable for flux calculations and only two traverses are included here, both showing fluxes around 200 kg/h. One of them is shown in Figure 24 and the details of both are given in Table 5. Due to the scarcity and lower reliability of the measurements, these should probably be seen as a rough estimate of the alkane flux.

Table 5 Summary of alkane emission transects from the Petrochemical Complex.

Region	Day	N	Start	Stop	Mean (kg/h)	SD (kg/h)	WS (m/s)	Range WD (deg)	
PC									
	120509	1	155848	160342	236.9	-	2.4	42	42
	120510	1	141814	142508	194.3	-	2.4	93	93
Total		**2**	**141814**	**160342**	**215.6**	**30.2**	**2.4**	**42**	**93**

5.1.3 Nitrogen dioxide (NO_2)

The Mobile DOAS measurements showed no signs of SO_2 from the Petrochemical Complex during the campaign, but a steady NO_2 plume was detected at all times. Figure 25 shows one NO_2 traverse on the north side of the Complex. All NO_2 measurements are summarized in Table 6. The average NO_2 flux measured was 118 kg/h with a standard deviation of 33 kg/h.

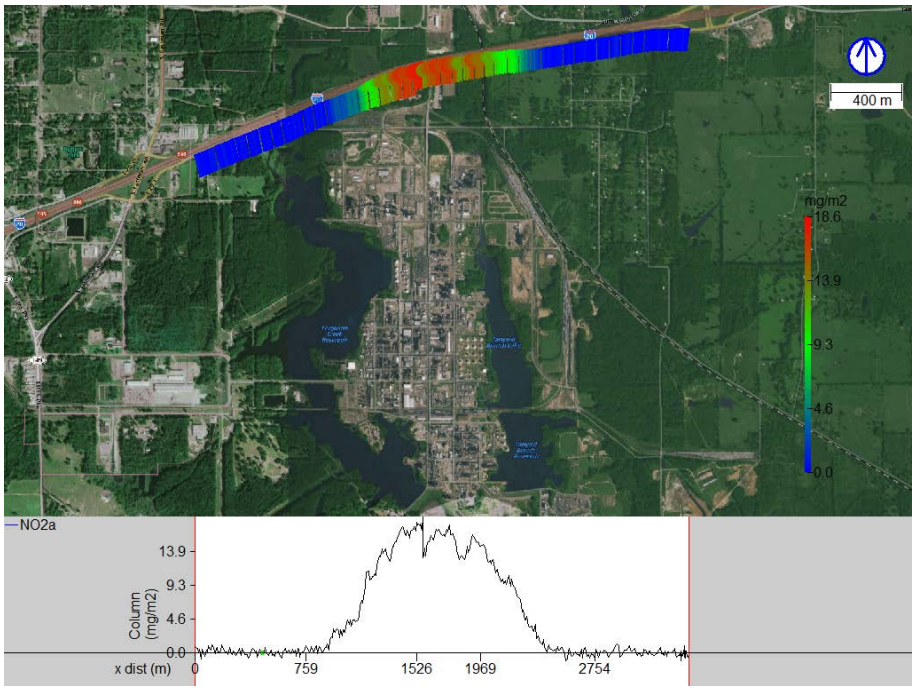

Figure 25 Mobile DOAS measurement of NO_2 north of the Petrochemical Complex on May 2, 2012, 14:35. Each measured spectrum is represented with a point, which color and size indicate the evaluated integrated vertical NO_2 column. The NO_2 column by distance driven through the plume is also shown in the lower part of the figure. A line from each point indicates the direction from which the wind is blowing.

Table 6 Summary of NO_2 emission transects from the Petrochemical Complex.

Region	Day	N	Start	Stop	Mean (kg/h)	SD (kg/h)	WS (m/s)	Range WD (deg)	
PC									
	120502	14	140255	181233	101.3	23.2	2.2	152	197
	120503	5	170908	184711	117.8	19.7	2.7	144	165
	120504	12	120106	184126	104.8	33.8	3.1	156	218
	120505	4	115057	141834	109.6	9.6	3.5	155	196
	120506	8	110755	164756	112.7	31.3	3.9	154	210
	120507	22	83019	181721	115.4	33.3	2.6	161	212
	120509	11	114401	171224	164.1	33.8	2.8	24	64
	120510	16	90205	144511	119.9	18.6	2.2	93	159
Total		**92**	**83019**	**184711**	**118.1**	**32.9**	**2.7**	**24**	**218**

5.1.4 Histograms

In total, there were 60-90 measurement traverses each for ethene, propene and NO_2 from the Petrochemical Complex. These were unevenly spread out over 8 days in a 9 day period and could be expected to be representative of at least this period. Figure 26 shows histograms for each of these species, visualizing the distribution of all the transects. In the histograms for ethene and propene, separate colors have been used for the measurements on the afternoon of May 7 and on May 10 respectively, since these days showed anomalies from the typical emissions seen. This clearly confirms the notion that something was different on these days. If the ethene measurements on the afternoon of May 7 are excluded from the data set, the average emission drops from 249 kg/h to 205 kg/h and the standard deviation drops from 130 kg/h to 57 kg/h. Similarly, the average propene emission drops from 211 kg/h to 172 kg/h and

the standard deviation from 122 kg/h to 77 kg/h, if the measurements on May 10 are excluded. Without these atypical measurements, the distributions look fairly Gaussian for ethene and NO_2. For propene, however, the emissions still seem to be somewhat unstable.

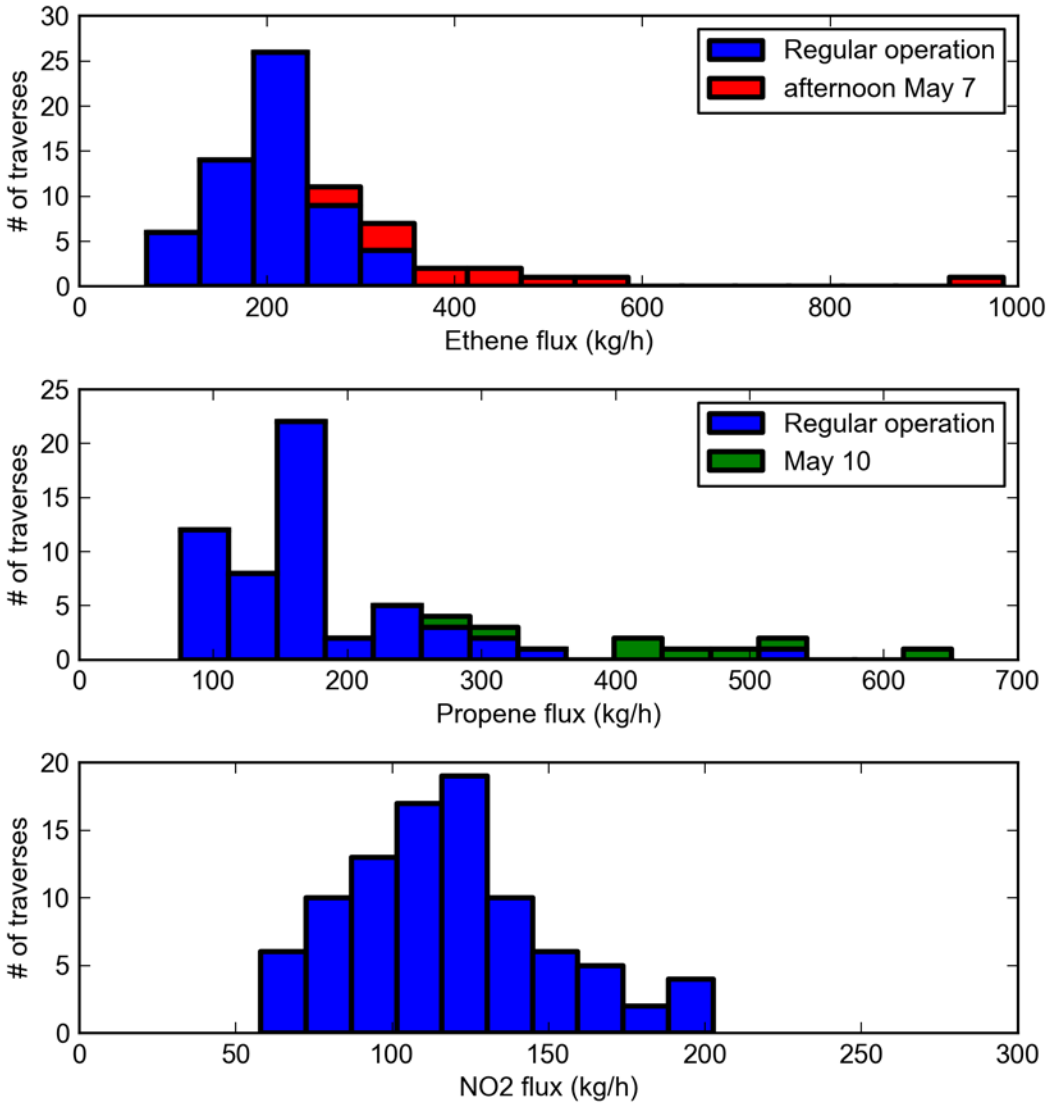

Figure 26 Histograms showing the distributions of fluxes measured for ethene, propene and NO_2 from the Petrochemical Complex. Ethene measurements in the afternoon of May 7 and propene measurements on May 10 are shown separately due to anomalous emission rates at these times.

7. Discussion

7.1 Comparison with emissions inventories

As mentioned in the introduction, the precursor to this study was one day of measurements at the Petrochemical Complex performed within the scope of a 2011 measurement study [Johansson 2011]. We can now compare the results from that day, the results from this longer study and the emissions reported to emission inventories. For this purpose, emission data for 2009 from the STARS (State of Texas Air Reporting System) emission inventory [STARS] have been retrieved for all companies located within the Petrochemical Complex. Figure 31 shows the locations and relative magnitudes of all emission point sources for ethene (cyan), propene (magenta), NO_x (blue) and SO_2 (red) within the Petrochemical Complex. These maps show that reported SO_2 emissions are negligible, which is consistent with the measurements finding no SO_2 plume from the Complex, and that of none of the other species seem to have their emission point concentrated in any single part of the Complex.

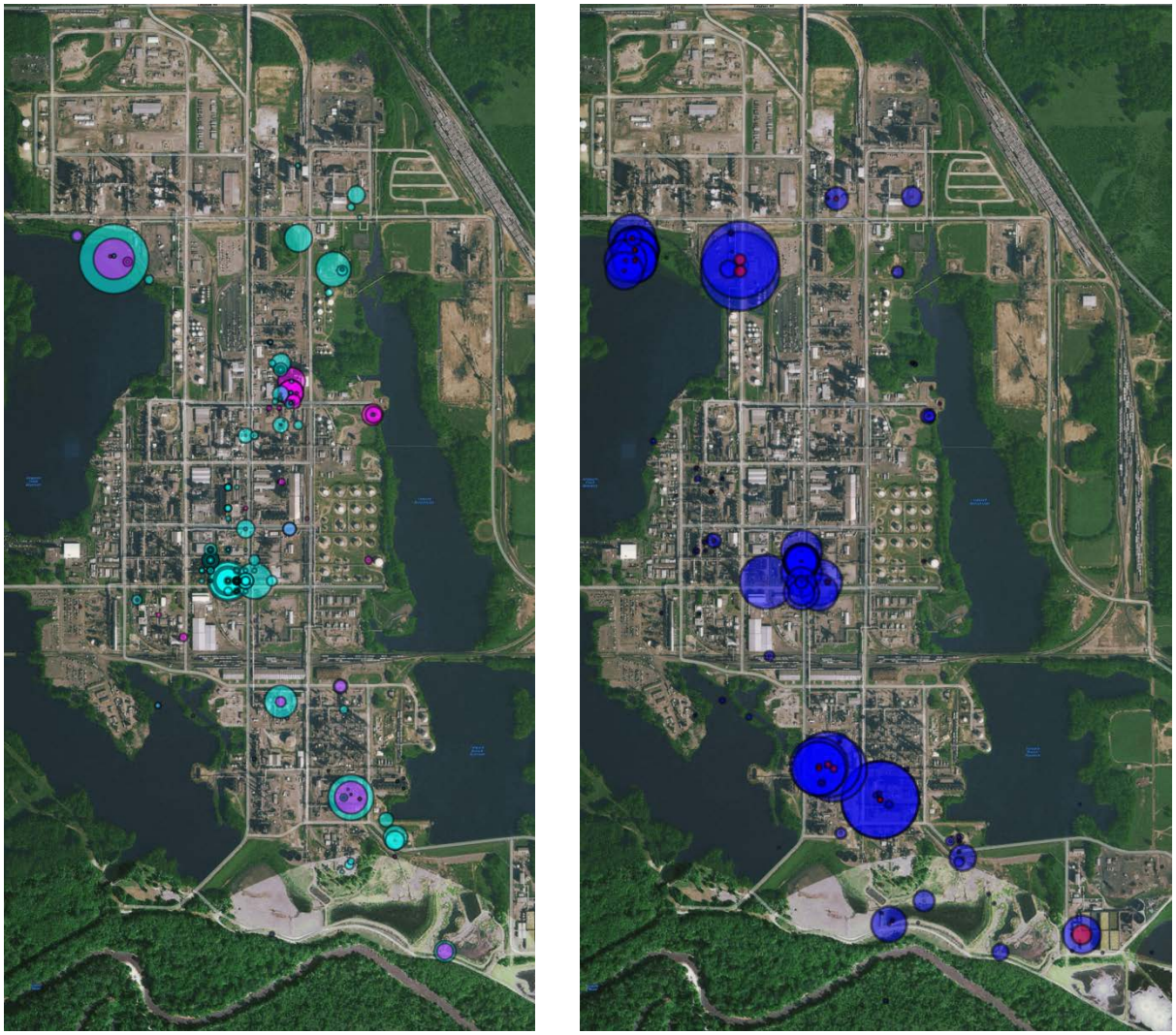

Figure 27 Maps showing the spatial distribution and relative magnitude of the reported emission point sources of the Petrochemical Complex. The left map shows ethene (cyan) and propene (magenta) sources while the right map shows NO_x (blue) and SO_2 (red) sources. The area of each circle is proportional to the emission rate of the source, but different scales were used for the two maps.

Table 11 compares the total emissions reported in the 2009 STARS inventory data to the measurement results for ethene, propene and NO_2. Measurements shown are the average fluxes measured during the one day of measurements in May 2011, the eight days of measurements in May 2012, and the eight days of measurement in May 2012 excluding the measurements suspected to be upset emissions. It should be noted that the emission inventories report NO_x emissions while only NO_2 is measured with Mobile DOAS. This comparison shows that the emissions measured in 2012 are significantly lower than those measured in 2011. However, the 2011 sample was only one measurement day and the 2012 study included days with elevated emissions of similar magnitude. Hence, the difference between the two studies cannot be taken as evidence of a trend towards lower emissions. Instead the larger measurement sample of the 2012 study should be viewed as more representative of the continuous emissions from the Petrochemical Complex.

Even though the emissions measured in 2012 were lower than those measured in 2011 a large discrepancy between measurements and inventories still persisted for ethene and propene. The difference for NO_2 was also fairly large but in this case the measurements showed lower emissions than the inventories. This is probably at least partly due to the inventory reporting NO_x and Mobile DOAS measuring NO_2. Not all NO_x emitted will be in the form of NO_2 at the point of measurement and exactly how much would vary depending on distance from the emission source and the plume chemistry.

Table 7 Comparison of results of SOF and Mobile DOAS measurements at the Petrochemical Complex in 2011 and 2012 to emissions reported to the 2009 STARS (State of Texas Air Reporting System) emission inventory. All emission rates in kg/h.

Species	**Measurements in 2011**	**Measurements in 2012**	**Measurements in 2012 without upsets**	**STARS emission inventory data 2009**
Ethene	452	249	205	113
Propene	282	211	172	32
NO_2	176	118	118	(NO_x) 207

7.2 Spatial distribution of emissions

One of the objectives of this study was to try to pinpoint the locations of the largest emission sources within the Petrochemical Complex. This is a task that increases in difficulty with the distance from the sources to the point of measurement and with the uncertainty of the wind direction. Preferably, this task is best achieved by measuring on the inside of a site, but such measurement requires permission from and coordination with the companies operating the plants and is usually a time consuming endeavour. Such measurements were not possible within the scope of this study. However, the typical measurement distance in this study, 1-3 km, is still close enough so that at least some information about the spatial distribution of the emission sources should be retrievable from measurements at a site of this size. Matters are, however, complicated by the fact that one wind direction (southerly) dominated the campaign to such a large extent and that the different facilities in the Complex are nearly lined up along this direction.

Figure 32 and Figure 33 show a composite plot of the measured plume profiles from the measurement transects from Figure 19 to Figure 23 for ethene and propene respectively. For each of the plume profiles the position of the maximum column have been traced back along the wind direction and the approximate area where they meet has been circled. The two figures look fairly similar since the same transects have been used and since the ethene and propene plume profiles were generally closely correlated. In both figures the same approximate area in the central or slightly south of central part of the Complex is circled. This seems to be the area dominating both the ethene and propene emissions. The difference that can be seen between the figures is that for propene the peak in the profile is more narrow around the maximum, indicating that emissions from other parts of the Complex are significantly smaller. For ethene on the other hand, the peak is less narrow and has a distinct tail, seen most clearly in the measurements on the west and southwest side of the Complex. This tail seem to indicate that there are also significant ethene emissions north of the central area.

It should be noted that this analysis would not fit with every measurement traverse in the study. For some traverses, tracing the maximum back along the wind direction would not intersect the area circled in Figure 32 and Figure 33. There is no single area within the Petrochemical Complex that would fit as the dominant source for each measurement traverse. The obvious reason for this is the errors in the wind direction assumed. These errors affect this type of analysis much more than they affect the flux calculation, due to the long distance from the source to the measurement point. The traverses used for this analysis were, after careful inspection of all traverses, chosen to represent the most typical traverses from different directions. However, this of course involved a certain amount of subjectivity. A more thorough analysis might be achieved using all traverses in some kind of statistical approach.

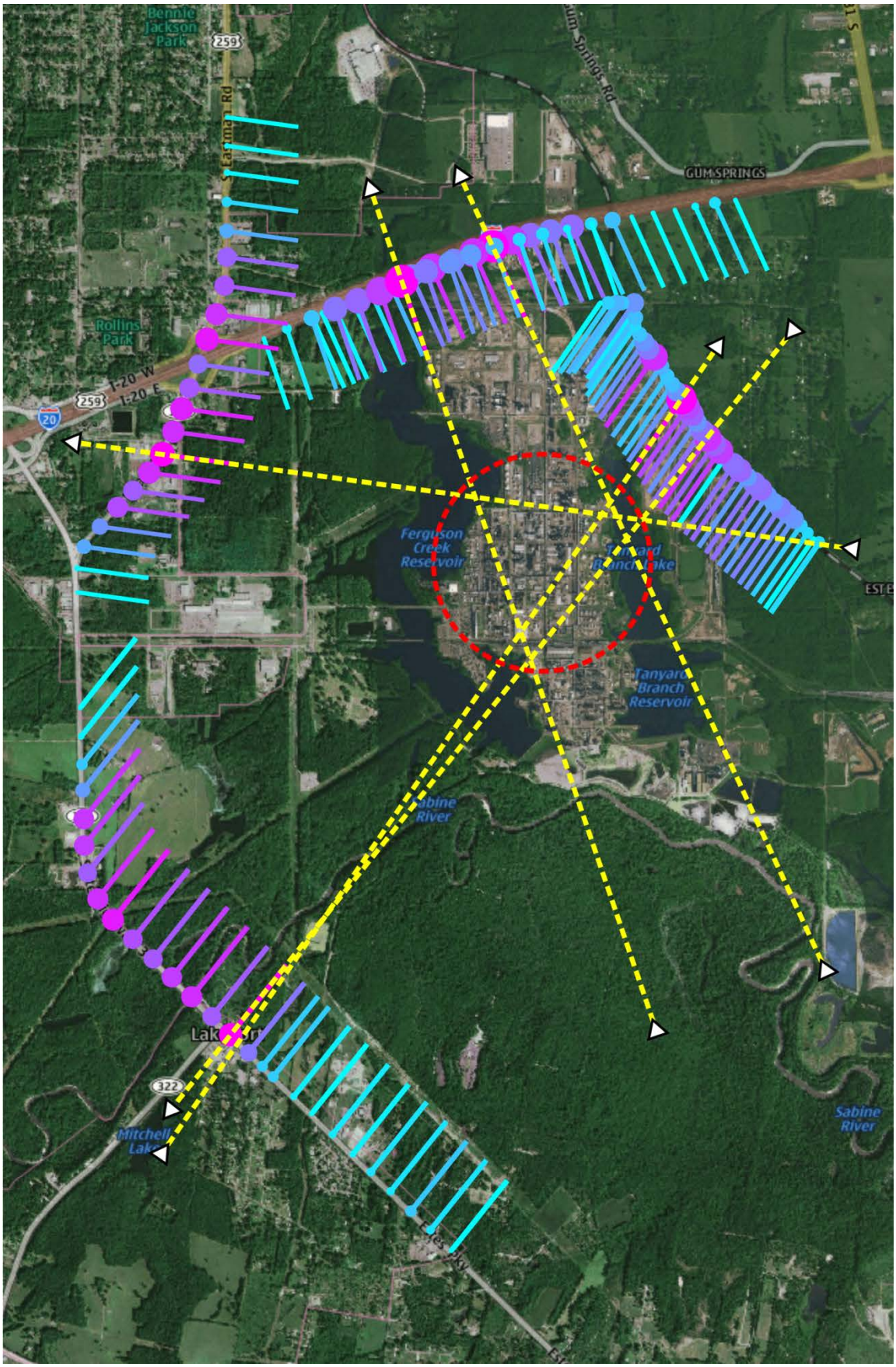

Figure 28 The ethene plume profiles for the five traverses in Figure 19 to Figure 23 shown together with dashed yellow lines tracing the point of maximum ethene column back along the wind direction. The dashed red circle shows the approximate area that all the yellow lines pass through.

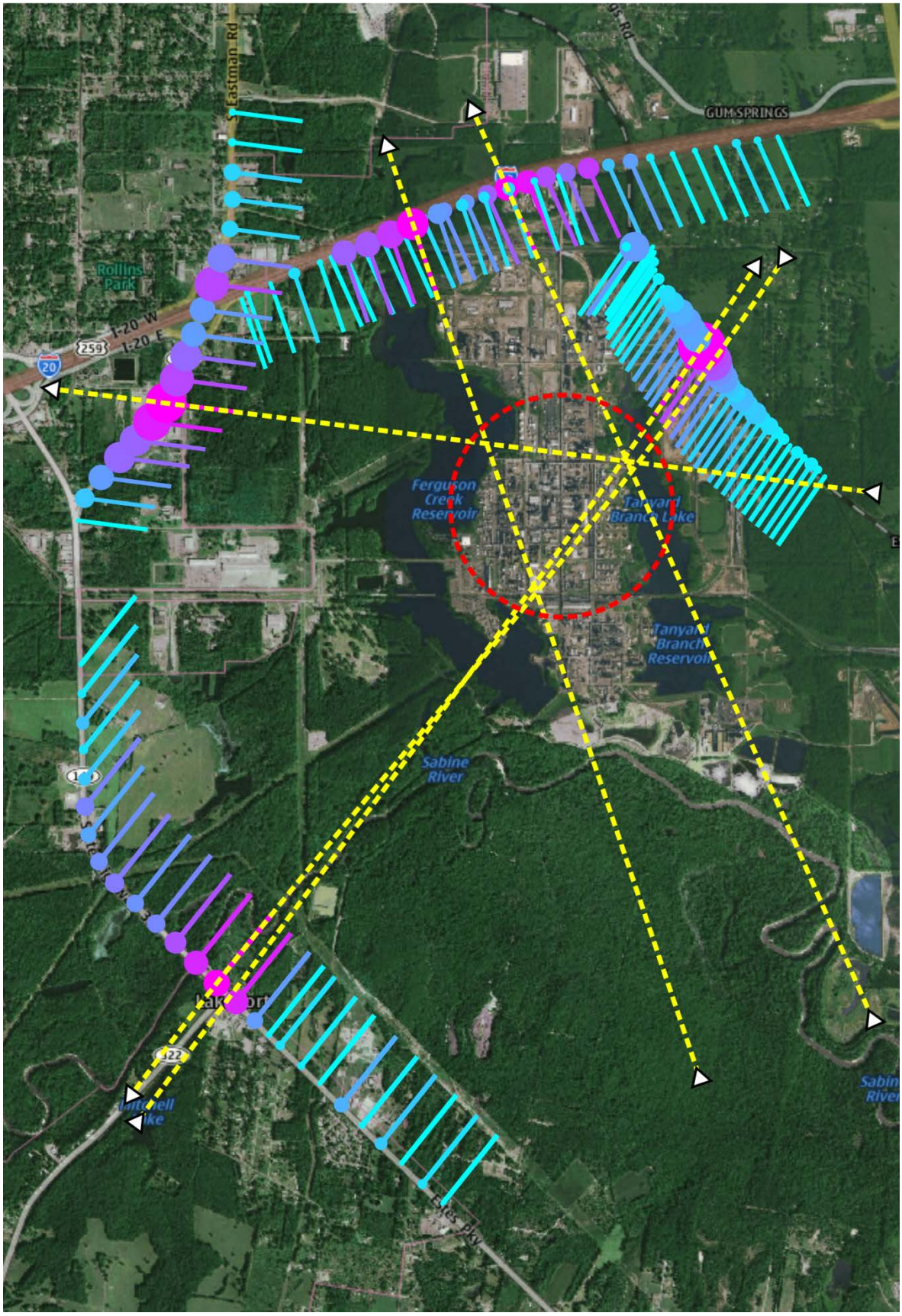

Figure 29 The propene plume profiles for the five traverses in Figure 19 to Figure 23 shown together with dashed yellow lines tracing the point of maximum ethene column back along the wind direction. The dashed red circle shows the approximate area that all the yellow lines pass through.

8. Acknowledgements

This work was funded by the state of Texas through the East Texas Council of Governments (ETCOG) under the technical direction of Northeast Texas Air Care (NETAC).

9. References

Allen, D.T. and V.M. Torres, 2010 TCEQ Flare Study Project, Final Report. 2011.

Arnold S.R., Methven J., Evans M.J., Chipperfield M.P., Lewis A.C., Hopkins J., McQuaid J.B., Watson N., Purvis R.M., Lee J.D., Atlas E.L., Blake D.R., Rappenglück B. (2007): Statistical inference of OH concentrations and air mass dilution rates from successive observations of nonmethane hydrocarbons in single air masses, *J. Geophys. Res.*, 112, D10S40, doi:10.1029/2006JD007594

Babilotte, A., Green, R., Hater, G., Watermolen, T., Staley, B., 2009, Field intercomparison of methods to measure fugitive methane emissions. Proceedings Sardinia 09 Twelfth International Waste Management and Landfill Symposium, CISA Environmental Sanitary Engineering Centre, Cagliari, Italy.

Bar-Ilan A. et al. (2008a), Development of baseline 2006 emissions from oil and gas activity in the Denver-Julesburg Basin, WRAP Phase III report, 34p, available at http://www.wrapair.org/forums/ogwg/PhaseIII_Inventory.html.

Bar-Ilan A. et al. (2008b), Development of the 2010 oil and gas emissions projections for the Denver-Julesburg Basin, WRAP Phase III report, 26p, available at http://www.wrapair.org/forums/ogwg/PhaseIII_Inventory.html.

Bogumil, K. et al., 2003, Measurements of Molecular Absorption Spectra with the SCIAMACHY PreFlight Model: Instrument Caracterization and Reference Data for Atmospheric Remote-Sensing in the 230–2380 nm Region, J. Photoch. Photobio. A, 157, 167–184

Buhr, M., Alvarez, S., Kauffmann, L., Shauck, M., Zanin, G., Alkene/NOy Emission Ratios observed from the Baylor Aztec during the 2006 TexAQS II study and Comparison with results obtained during 2001–2002, Rapid science synthesis workshop, Austin, october 12, 2006

Burrows, J.P et al., 1999, Atmospheric Remote-Sensing Reference Data from GOME: 2. Temperature-Dependent Absorption Cross Sections of O3 in the 231–794 nm Range, Journal of Quantitative Spectroscopy and Radiative Transfer 61, 509–517

Börjesson, G., J. Samuelsson, J. Chanton, R. Adolfsson, B. Galle, and B.H. Svensson. 2009. A national landfill methane budget for Sweden based on field measurements, and an evaluation of IPCC models. Tellus, 61B: 424–435.

Cantrell CA, Davidson JA, McDaniel AH, Shetter RE, Calvert JG. 1990, Temperature dependent formaldehyde cross sections in the near-ultraviolet spectral region. J Phys Chem, 94:3902–8.

De Gouw, J.A., et. al. (2009), Airborne Measurements of Ethene from Industrial Sources Using Laser Photo-Acoustic Spectroscopy, Environmental Science and Technology, 43, 2437–2442.

ERG, Forth Natural gas Air Quality Study Final Report, 2011, www.forthworthgov.org

Fayt, C. and Van Roozendael, M., 2001. QDOAS 1.00 Software User Manual, BIRA-IASB.

Fish, D.J. and Jones, R.L., 1995. Rotational Raman scattering and the ring effect in Zenith-sky spectra. Geophysical Research Letters, 22(7): 811–814.

Galle, B.; Mellqvist, J., et al., Ground Based FTIR Measurements of Stratospheric Trace Species from Harestua, Norway during Sesame and Comparison with a 3-D Model, JAC, 1999, 32, no. 1, 147–164.

Galle, B., J. Samuelsson, B.H. Svensson, G. Börjesson, "Measurements of methane emissions from landfills using a time correlation tracer method based on FTIR absorption spectroscopy." Environ. Sci. Technol. 35: 21–25. 2001.

Galle, B., Oppenheimer, C., Geyer, A., McGonigle, A.J.S., Edmonds, M. and Horrocks, L., (2002), A miniaturised ultraviolet spectrometer for remote sensing of SO2 fluxes: A new tool for volcano surveillance, Journal of Volcanology and Geothermal Research, 119 241–254

Gratien, A. et al (2007), UV and IR Absorption Cross-sections of HCHO, HCDO, and DCDO, J. Phys. Chem. A, 111, 11506–11513

Grenfell R.J.P., Milton M.J.T., Harling A.M., Vargha G.M., Brookes C., Quincey P.G., Woods P.T. (2010): Standard mixtures of ambient volatile organic compounds in synthetic and whole air with stable reference values, *J. Geophys. Res*, 115, D14302, doi:10.1029/2009JD012933

Griffith D.W.T., Synthetic calibration and quantitative analysis of gas-phase FT-IR spectra. Applied Spectroscopy, 1996. 50(1): p. 59–70.

Heckel, A., A. Richter, T. Tarsu, F. Wittrock, C. Hak, I. Pundt, W. Junkermann, and J.P. Burrows, MAX-DOAS measurements of formaldehyde in the Po-Valley, Atmospheric Chemistry and Physics, 5, 909–918, 2005.

Hermans, C.et al., Absorption cross-sections of atmospheric constituents: NO_2, O_2, and H_2O, Environ. Sci. Pollut. R. , 6, 151–158, 1999.

Hurley, P.J., Physick W.L., and Luhar A.K., TAPM: A practical approach to prognostic meteorological and air pollution modelling. Environmental Modelling and Software, 2005. 20(6): p. 737.

Johansson, J., Mellqvist, J., Samuelsson, J., Offerle, B., Rappenglück, B., Anderson, D., Lefer, B., Alvarez, S. and Flynn, J. (2011), Quantification of industrial emissions of VOCs, NO2 and SO2 by SOF and Mobile DOAS, AQRP Project 10-006, AQRP report., Texas.

Johansson, M., C. et al, 2009, Mobile mini-DOAS measurement of the outflow of NO2 and HCHO from Mexico City, Atmos. Chem. Phys., 9, 5647–5653

Kihlman, M. (2005a), Application of solar FTIR spectroscopy for quantifying gas emissions, Technical report No. 4L, ISSN 1652-9103, Department of Radio and Space Science, Chalmers University of Technology, Gothenburg, Sweden.

Kihlman, M., J. Mellqvist, and J. Samuelsson (2005b), Monitoring of VOC emissions from three refineries in Sweden and the Oil harbor of Göteborg using the Solar Occultation Flux method, Technical report, ISSN 1653 333X, Department of Radio and Space, Chalmers University of Technology, Gothenburg, Sweden.

Koppmann R., Johnen F.J., Khedim A., Rudolph J., Wedel A., Wiards B. (1995): The influence of ozone on light nonmethane hydrocarbons during cryogenic preconcentration, *J. Geophys. Res.*, **100**, 11383–11391.

Leuchner M., Rappenglück B. (2010): VOC Source-Receptor Relationships in Houston during TexAQS-II, *Atmos. Environ.*, **44**, 4056–4067, doi:10.1016/j.atmosenv.2009.02.029

Mellqvist, J., Application of infrared and UV-visible remote sensing techniques for studying the stratosphere and for estimating anthropogenic emissions, doktorsavhandling, Chalmers tekniska högskola, Göteborg, Sweden, 1999a

Mellqvist, J och Galle, B., Utveckling av ett IR absorptionssystem användande solljus för mätning av diffusa kolväteemissioner, Rapport till Preems miljöstiftelse juli 1999b.

Mellqvist, J., Arlander, D. W., Galle, B. and Bergqvist, B., Measurements of Industrial Fugitive Emissions by the FTIR-Tracer Method (FTM), IVL report, 1995, B 1214.

Mellqvist, J., Flare testing using the SOF method at Borealis Polyethylene in the summer of 2000. 2001, Chalmers University of Technology. (Available at www.fluxsense.se)

Mellqvist, J., J. Samuelsson, C. Rivera, B. Lefer, and M. Patel (2007), Measurements of industrial emissions of VOCs, NH_3, NO_2 and SO_2 in Texas using the Solar Occultation Flux method and mobile DOAS, Project H053.2005, Texas Environmental Research Consortium., Texas. (http://www.harc.edu/projects/airquality/Projects/Projects/H053.2005)

Mellqvist, J.,Berg N. and Dan Ohlsson, 2008a, Remote surveillance of the sulfur content and NOx emissions of ships, Second international conference on Harbours, Air Quality and Climate Change (HAQCC), Rotterdam.

Mellqvist, J., Johansson, J. ,Samuelsson, J., Rivera, C., Lefer, B. and S. Alvarez (2008b), Comparison of Solar Occultation Flux Measurements to the 2006 TCEQ Emission Inventory and Airborne Measurements for the TexAQS II, Project No. 582-5-64594-FY08-06 , TCEQ report., Texas. (available at http://www.tceq.state.tx.us/assets/public/implementation/air/am/contracts/reports/da/20081108-comparison_solar_occultation_flux_measurements.pdf)

Mellqvist, J., et al. (2009a), Emission Measurements of Volatile Organic Compounds with the SOF method in the Rotterdam Harbor 2008, available at www.fluxsense.se

Mellqvist, J., J. Samuelsson, J. Johansson, C. Rivera, B. Lefer, S. Alvarez, and J. Jolly (2010), Measurements of industrial emissions of alkenes in Texas using the solar occultation flux method, J. Geophys. Res., 115, D00F17, doi:10.1029/2008JD011682.

Methven J., Arnold S.R., Stohl A., Evans M.J., Avery M., Law K., Lewis A.C., Monks P.S., Parrish D., Reeves C., Schlager H., Atlas E., Blake D., Coe H., Cohen R.C., Crosier J., Flocke F., Holloway J.S., Hopkins J.R., Hübler G., Lee J.D., Purvis R., Rappenglück B., Ryerson T.B., Sachse G.W., Singh H., Watson N., Whalley L., Williams P. (2006): Establishing Lagrangian connections between observations within air masses crossing the Atlantic during the International Consortium for Atmospheric Research on Transport and Transformation experiment, *J. Geophys. Res.*, 111, D23S62, doi:10.1029/2006JD007540

Plass-Dülmer C., Schmidbauer N., Slemr J., Slemr F., D'Souza H. (2006): The European Hydrocarbon Intercomparison Experiment AMOHA Part 4: Canister Sampling of Ambient Air, *J. Geophys. Res.*, 111, D4, D04306, doi:10.1029/2005JD006351

Platt, U., D. Perner, and H.W. Pätz, Simultaneous Measurement of Atmospheric CH2O, O3 and NO2 by Differential Optical Absorption, Journal of Geophysical Research, 84 (C10), 6329–6335, 1979.

Rappenglück B., Schmitz R., Bauerfeind M., Cereceda-Balic F., v. Baer D., Jorquera H., Silva Y., Oyola P. (2005): An urban photochemistry study in Santiago de Chile, *Atmos. Environ.*, 39, 2913–2931, doi:10.1016/j.atmosenv.2004.12.049

Rappenglück B., Apel E., Bauerfeind M., Bottenheim J., Brickell P., Čavolka P., Cech J., Gatti L., Hakola H., Honzak J., Junek R., Martin D., Noone C., Plass-Dülmer Ch., Travers D., Wang T (2006): The first VOC intercalibration exercise within the Global Atmosphere Watch (GAW), *Atmos. Environ.*, 39, 2913–2931, doi:10.1016/j.atmosenv.2004.12.049

Rappengluck, B. et al, 2008a, Analysis of Primary vs. Secondary Fraction of Formaldehyde Houston Area During TexAQS-II, 10th Conference on Atmospheric Chemistry conference, The 88th Annual Meeting (20–24 January 2008), AMS,

Rappenglück, B et al, (2008b): In‐Situ Ground‐Based and Airborne Formaldehyde Measurements during the TRAMP Study; Atmos.Environ., submitted.

Rinsland, C. P., R. Zander, and P. Demoulin (1991), Ground-based infrared measurements of HNO3 total column abundances: long-term trend and variability, *J. Geophys. Res.*, *96*, 9379–9389.

Rivera, C. et al., (2010), Quantification of NO2 and SO2 emissions from the Houston Ship Channel and Texas City during the 2006 Texas Air Quality Study, J. Geophys. Res., 115, D08301, doi:10.1029/2009JD012675

Rivera , C., Application of Passive DOAS using Scattered Sunlight for quantification of gas emission from anthropogenic and volcanic sources (2009a), Dissertation, ISBN 978-91-7385-317-0, ISSN 0346

Rivera, C., J.A. Garcia, B. Galle, L. Alonso, Y. Zhang, M. Johansson, M. Matabuena, and G. Gangoiti (2009b), Validation of optical remote sensing measurement strategies applied to industrial gas emissions, Int. J. Remote Sens., vol 30, no 12, p3191–3204.

Rivera, C., et al. (2009c),Tula industrial complex (Mexico) emissions of SO2 and NO2 during the MCMA 2006 field campaign using a mobile mini_DOAS system, Atmos. Chem. Phys., 9, 6351–6361, 2009.

Rothman et al. (2003), HITRAN 2000, Journal of Quantitative Spectroscopy and Radiative Transfer, vol. 82, pp. 5–44.

Ryerson, T. B., et al. (2003), Effect of petrochemical industrial emissions of reactive alkenes and NOx on tropospheric ozone formation in Houston, Texas, J. Geophys. Res., 108(D8), 549 4249, doi:10.1029/2002JD003070.

Samuelsson, J., Börjesson, G., Svensson, B., Galle, B., Metan från avfallsupplag i Sverige (Methane from landfills in Sweden), final report to the Swedish Energy Agency, projekt nr P10856-4, December 2005a. In Swedish (www.stem.se), can be ordered from Studsviksbiblioteket, 611 82 Nyköping, Sweden, www.lib.kth.se/SB/service/stemavf.html.

Samuelsson, J., et. al., VOC measurements of VOCs at Nynas Refinery in Nynäshamn 2005b *(Utsläppsmätningar av flyktiga organiska kolväten vid Nynas Raffinaderi i Nynäshamn 2005, in Swedish*), Bitumen refinery official report to provincial government 2005, Available at: http://www.fluxsense.se

Schürmann G., Schäfer K., Jahn C., Hoffmann H., Bauerfeind M., Fleuti E., Rappenglück B. (2007): The Impact of NO_x, CO and VOC Emissions on the Air Quality of the Airport Zurich, *Atmos. Environ.*, 41, 103–118, doi:10.1016/j.atmosenv.2006.07.030

Sharpe, S., et al. (2004), Gas-Phase Databases for Quantitative Infrared Spectroscopy, *Applied Optics, 58*(12).

Slemr J., Slemr F., Partridge R., D´Souza H., Schmidbauer N. (2002): Accurate measurements of hydrocarbons in the atmosphere (AMOHA): three European intercomparisons, *J. Geophys. Res.*, 107, D19, 4409, doi:10.1029/2001JD001357

STARS, Emission inventory data extracted by John Jolly of the Texas Commission on Environmental Quality (TCEQ) from the TCEQ's State of Texas Air Reporting System (STARS) database, on Sept 28, Oct 3, and Oct 4, 2011.

Sullivan, D., et al, Oil and Gas Emissions in the DFW Region, University of Austin report , TCEQ Grant Activities No. 582-8-86245-FY09-03 , Jan , 2010

Taylor, B., and C. Kuyatt, 1994. “Guidelines for Evaluating and Expressing the Uncertainty of NIST Measurement Results.” NIST Technical Note 1297 1994 edition. Gaithersburg, MD.

Thoma, E. et al. (2009), Development of EPA OTM 10 for Landfill Applications, in print, Journal of Environmental Engineering

Tucker, S., Marine boundary Layer dynamics and heights during TexAQS 2006: HRDL measurements from the RV Brown, Principal Findings Data Analysis Workshop TexAQS II, Austin, May 29–June 01, 2007. (available at www.tceq.state.tx.us)

URS Corporation, 2004. Passive FTIR Phase I Testing of Simulated and Controlled Flare Systems. Final report prepared for the Texas Commision on Environmental quality (TCEQ), 12100 Park 35 Circle, Austin, TX 78753

Vandaele A.C., C. Hermans, P.C. Simon, M. Carleer, R. Colin, S. Fally, M.F. Mérienne, A. Jenouvrier, and B. Coquart, Measurements of the NO2 absorption cross-section from 42000 cm-1 to 10000 cm-1 (238–1000 nm) at 220 K and 294 K, J.Q.S.R.T., 59, 171–184 (1998)

Veillerot M., Locoge N., Galloo J.C., Guillermo R. (1998): Multidimensional capillary gas chromatography for the monitoring of individual non-methane hydrocarbons in air, *Analysis Magazine*, **26**, M38–M43.

Walmsley, H. L., and S. J. O'Connor (1998), The accuracy and sensitivity of infrared differential absorption lidar measurements of hydrocarbon emissions from process units. *Pure Appl. Opt.*, *7*, 907–925.

Wert, B. P., et al. (2003), Signatures of terminal alkene oxidation in airborne formaldehyde 571 measurements during TexAQS 2000, J. Geophys. Res., 108(D3), 4104, doi:10.1029/2002JD002502, 2003.

Winkler J., Blank P., Glaser K., Habram M., Jambert C., Jaeschke W., Konrad S., Kurtenbach R., Lenschow P., Perros P., Pesch M., Prümke H.-J., Rappenglück B., Schmitz T., Slemr F., Volz-Thomas A. and Wickert B. (2002): Nonmethane hydrocarbon measurements in BERLIOZ: Characterization of the ground-based measurement sites and emission ratios derived from airborne measurements, *J. Atmos. Chem.*, 42, 465–492